A model analysis of the tropical South Atlantic Ocean tropospheric ozone maximum: The interaction of transport and chemistry

W. J. Moxim and H. Levy II

Geophysical Fluid Dynamics Laboratory, Princeton University, Princeton, New Jersey

Abstract. The meteorological and photochemical nature of the South Atlantic Ocean tropospheric column ozone maximum is examined by analyzing the Geophysical Fluid Dynamics Laboratory (GFDL) Global Chemical Transport Model (GCTM) simulation during the Southern Hemisphere late winter. An ozone maximum of greater than 40 Dobson units is produced by the GCTM over the South Atlantic Ocean. The model is evaluated against available meteorological and ozone data and found to be in good qualitative agreement with observed wind fields, satellite measurements of tropospheric column ozone, tropospheric column ozone produced from ozonesonde data, and vertical profiles from ozonesondes. A quantitative analysis is performed over an area of the South Atlantic Ocean essentially devoid of local NO_x sources and for a time, September, when the regional tropospheric ozone mass is at a maximum. The tropospheric mass of reactive nitrogen transported into the region is a result of source contributions from lightning (49%), biomass burning (36%), and 15% from the remaining NO_x sources (fossil fuel plus biogenic plus stratosphere plus aircraft). Even with the removal of biomass burning NO_x from the ozone photochemical system, the GCTM still produces an oceanic tropospheric column ozone maximum, suggesting the ozone phenomenon existed before agricultural burning by humans. The structure of clean air CO/CH_4 net chemistry consists of ozone production in the upper troposphere (+2.2 Tg/month), weak destruction in the middle troposphere (-1.8 Tg/month), and strong destruction in the lower troposphere (-4.2 Tg/month). Through photochemistry, the two largest NO_x sources help control the vertical profile of ozone with lightning dominating in the upper troposphere, while the relative importance of biomass burning is virtually constant throughout the troposphere. A mass budget analysis of ozone over the tropospheric South Atlantic Ocean reveals that net mass transport of ozone into the domain is nearly balanced by net chemical destruction and deposition and that the mass transport into and out of the region are comparable to the chemical production and destruction terms. The three-dimensional circulation governing the ozone vertical structure is one of horizontal mass convergence and net chemical production supplying ozone to the upper troposphere which is fluxed downward by subsidence and removed in the boundary layer by net chemical destruction, deposition, and horizontal mass divergence.

1. Introduction

The meteorology of the subtropics and tropics of the South Atlantic Ocean (SAO) exhibits a unique circulation regime which is quasi-stationary in space and time with essentially desert-like precipitation (0.1 to 1.0 mm/d) [*Lockwood*, 1974; *Hoflich*, 1984]. The basic flow field features a surface anticyclone anchored off the African coast near 30°S which produces southeast trade winds from the west coast of Africa to the Intertropical Convergence Zone (ITCZ) north of the equator, and this divergent anticyclonic outflow is supported by significant regional subsidence [*Krishnamurti et al.*, 1993]. In addition, work done by *Kidson* [1975] showed that this region undergoes a Walker-type circulation with rising motion over the continents of South America and Africa, convergent flow

in the upper troposphere over the South Atlantic, and subsequent sinking [*Newell*, 1979].

The implications of this circulation on the regional distribution of ozone was first hinted at when aircraft flights in the 1960s and 1970s found significantly higher values of ozone over the upper troposphere of the tropical Atlantic as compared with the tropical Pacific [*Machta et al.*, 1969; *Pratt and Falconer*, 1979; *Newell and Wu*, 1985]. Also, in the 1980s, analysis of ozonesonde data at Natal, Brazil, depicted higher amounts of ozone in the southern tropics than those found in the northern tropics with austral spring concentrations as high as summer values found in northern midlatitudes [*Kirchhoff*, 1984; *Logan and Kirchhoff*, 1986]. During this time the role of nitrogen oxides in the production of ozone and the concentration of tropospheric OH was being refined [*Chameides and Walker*, 1973; *Fishman et al.*, 1979; *Crutzen*, 1979], and measurements were made of the distribution and strengths of the NO_x sources, where in the tropics, biomass burning plays a major role [*Seiler and Crutzen*, 1980; *Logan et al.*, 1981; *Logen*, 1983]. The actual transport of biomass burning prod-

ucts was indicated by the work of *Andreae* [1983] in which aerosols of the type dominated by burning of biomass were detected off the coast of Brazil. Additionally, *Logan and Kirchhoff* [1986], speculated that the high concentrations of ozone in the upper troposphere over Natal are the result of the mixing of ozone-rich boundary layer air over Brazil to the free troposphere where subsequent westerlies above 400 mbar provide transport to Natal.

The real surprise as to the extent of the influence of biomass burning on the SAO region was revealed by the pioneering work on the distribution of tropospheric column ozone from satellite data (referred to as the tropospheric ozone residual (TOR)) [*Fishman et al.*, 1990, 1991]. This technique allowed for the first time an examination of horizontal tropospheric gradients over much of the globe. In particular, Fishman's analysis detected a large ozone maximum over the SAO during the austral spring with a closed contour of greater than 40 Dobson units (DUs) over the ocean isolated from the continental biomass burning regions of both Africa and South America. The analysis clearly indicated that an interaction of atmospheric transport of ozone and its precursors along with in situ photochemistry was somehow focused in this remote region. This finding concentrated interest in the region and eventually led to an intensive field mission, the Southern Tropical Atlantic Region Experiment (STARE), consisting of two campaigns; Transport and Atmospheric Chemistry Near the Equator - Atlantic (TRACE-A) and Southern African Fire-Atmosphere Research Initiative (SAFARI). It was conducted in September-October 1992 and provided an extensive data set from which the meteorology and atmospheric chemistry of the tropical SAO could be explored [*Andreae et al.*, 1996].

During the early 1990s the first attempts to examine the SAO ozone maximum utilizing numerical models were performed. To investigate the role of ozone transport, *Krishnamurti et al.* [1993] used the Florida State University global spectral model to simulate the evolution of tropospheric ozone during October. Starting from a height-dependent, zonally symmetric ozone distribution and neglecting photochemistry, they found that the model dynamics produced tropospheric column ozone patterns somewhat similar to the observed, suggesting that general synoptic transport tends to accumulate ozone off the west coast of southern Africa. In a later study, *Krishnamurti et al.* [1996] further emphasized the role transport plays in accumulating ozone and its precursors in the SAO by demonstrating that a "dynamics alone" 1-week model integration produced a correlation coefficient of roughly 0.8 with observational total atmospheric ozone from the Total Ozone Mapping Spectrometer (TOMS). *Richardson* [1994] and *Olson* [1996] also examined ozone transport to the SAO using the Geophysical Fluid Dynamics Laboratory (GFDL) global transport model. By constraining the inert tracer (no chemistry) to reproduce observed seasonal ozone increases over continental burning regions, integrating the model over an entire year, and comparing with available satellite residuals, it was demonstrated that while the model could reasonably reproduce the shape of the seasonal cycle, it was able to account for no more than 25% of the seasonal increase over the SAO. Also, utilizing nearby ozonesonde data as a surrogate for the vertical distribution of the tropospheric column ozone and comparing with the simulated ozone profile, it was found that the largest model deficits occurred in the upper troposphere. Assuming that the underestimate resulted from the lack of net photochemical production of ozone, the results

showed that a net source of ~5 ppbv per day in the upper troposphere over the SAO was needed to make up the deficit, which was not unreasonable when compared to current estimates from observations and models [e.g., *Jacob et al.*, 1996; *Pickering et al.*, 1996; *Thompson et al.*, 1996; *Klonecki and Levy*, 1997; *Roelofs et al.*, 1997].

In 1996 the results of the TRACE-A and SAFARI studies were published [*Fishman et al.*, 1996; *Lindesay et al.*, 1996]. The findings indicated that a complex mix of meteorology and photochemistry produces the SAO maximum. In this region, continental biomass burning precursors play a dominant role in SAO ozone formation, meteorological transport accumulates pollutants in this region, and upper tropospheric net production of ozone from high concentrations of NO_x suggests rapid vertical mixing and/or production of NO_x from lightning. In addition, a later study by *Mauzerall et al.* [1998] utilizing TRACE-A data argued that ozone production in biomass burning plumes is sufficient to fully explain the observed enhancement in tropospheric ozone over the tropical South Atlantic during the dry season. While the intensive research on the TRACE-A and SAFARI data has provided exceptional qualitative insight into the mechanisms driving the SAO maximum, the data are still insufficient to separately analyze the roles of transport and chemistry quantitatively.

Another viable approach to investigating the SAO phenomenon would be the analysis of a successful simulation generated from a three-dimensional chemical/transport model. By providing a continuous set of data available at all grid points, a self-consistent budget analysis of chemistry and transport could be performed. *Roelofs et al.* [1997] used a coupled chemistry-general circulation model, European Center Hamburg Model, version 4 (ECHAM4) without non-methane hydrocarbons, to examine the tropical SAO. While the simulation was unable to produce a closed maximum of column ozone over the ocean and, due to model constraints, could not quantify the individual roles of NO_x sources, they inferred that photochemical production of ozone was mainly associated with biomass burning precursors. Their net photochemistry over the South Atlantic basin was in general agreement with TRACE-A results, showing net destruction in the lower troposphere (up to 4 ppbv per day), changing to weak production near 5 km with 1 to 2 ppbv per day production in the upper troposphere. They also found that model ozone transport out of the stratosphere was of minor importance. The chemical transport model, Model for Ozone and Related Chemical Tracers (MOZART), has also been used to simulate ozone and related species on a global scale [*Hauglustaine et al.*, 1998]. A world map of tropospheric column ozone simulated in MOZART depicts a reproduction of the SAO ozone maximum with values of 30-32 DU. However, the regional ozone budget was not analyzed.

In this study we present an analysis of the SAO ozone maximum produced by the GFDL Global Chemical Transport Model (GCTM). After comparing the ozone simulation with available observations from satellite and ozondesondes, as well as the model's meteorology with climatological flow fields, we examine the contribution of the individual NO_x sources to its vertical profile in the region. Next, we show how the elimination of a significant NO_x source changes the tropospheric column ozone distribution by altering its photochemistry and resulting vertical distribution. Additionally, we present a regional budget analysis for both NO_x and ozone which demonstrates the magnitude and role of photochemis-

try and transport, and then depict the three-dimensional mass transport and circulation of ozone produced by the GCTM.

2. Model Description

The GFDL GCTM has a horizontal grid size of ~265 km (2.4°x2.4° in the tropics and 3°-3.5°x2.4° in midlatitudes), and 11 (terrain-following) sigma levels in the vertical at standard pressures of 990, 940, 835, 685, 500, 315, 190, 110, 65, 38, and 10 mbar for a surface pressure of 1000 mbar, corresponding to standard heights of 0.08, 0.5, 1.5, 3.1, 5.5, 8.7, 12.0, 15.5, 18.8, 22.3, and 31.4 km. It is driven by 6-hour time-averaged winds, instantaneous temperature sampled every 6 hours, and a consistent total column precipitation field that were generated by a parent general circulation model (GCM) integrated for 1 year without diurnal insulation (see *Mahlman and Moxim* [1978, section 2] for a summary, and *Manabe et al.* [1974] and *Manabe and Holloway* [1975] for details). Therefore the GCTM cannot examine interannual variability or diurnal variations in the boundary layer (BL) due to daily solar heating. The transport portion of the model employs a numerical scheme which is fourth order in the vertical and second order in the horizontal, and its time and space resolution is sufficient to realistically reproduce synoptic-scale transport due to extratropical cyclones and their associated frontal systems [*Moxim*, 1990; *Moxim et al.*, 1996]. The model includes parameterizations designed to incorporate the effects of horizontal subgrid-scale transport, as well as vertical mixing by dry and moist convection (for details, see *Levy et al.* [1982, Appendix A], *Kasibhatla et al.* [1993, section 2], and *Levy et al.* [1999]).

The ozone simulation by the GCTM has been used and described in detail in previous studies [*Kasibhatla et al.*, 1996; *Klonecki and Levy*, 1997; *Levy et al.*, 1997; *Yienger et al.*, 1999; *Levy et al.*, 1999; *Galanter et al.*, 2000]. It consists of four major components: (1) irreversible transport of stratospheric ozone into the troposphere; (2) Photochemistry of the NO_x-CO/acetone-CH_4-O_3-H_2O system (hereafter described as CO/CH_4) throughout the free troposphere and unpolluted BL; (3) parameterized photochemical production of ozone in the polluted continental BL; and (4) seasonal and vegetation-dependent surface deposition of tropospheric ozone. The background CO/CH_4-based ozone chemical tendencies in each appropriate grid box are calculated every time step by an interpolation of values from precalculated tables [*Klonecki and Levy*, 1997] based on the model's instantaneous ozone levels and 6-hour sampled NO_x [*Levy et al.*, 1999] and CO levels [*Holloway et al.*, 2000] generated from previous GCTM simulations using the identical meteorology for transport, and monthly averaged H_2O concentrations from observations [*Oort*, 1983; *Soden and Bretherton*, 1996]. Pollution production of ozone in the BL and lower troposphere is determined by previously computed concentrations of NO_x and isoprene which act as surrogates for reactive hydrocarbons. On the basis of empirical relationships, ozone is produced when either NO_x exceeds 200 parts per trillion by volume (pptv) or isoprene exceeds 100 pptv and NO_x exceeds 50 pptv (see *Kasibhatla et al.* [1996], *Levy et al.* [1997], and *Yienger et al.* [1999] for a more complete discussion). Both the CO/CH_4 and pollution chemistries include synoptic-scale fluctuations of the ozone precursors.

The GCTM simulation of reactive nitrogen [NO_y] has been presented in earlier works [*Moxim et al.*, 1996; *Levy et al.*,

1999]. The model transports three species: nitrogen oxides ($NO + NO_2 + NO_3 + N_2O_5$), nitric acid ($HNO_3$), and peroxyacetyl nitrate (PAN) and includes six global reactive nitrogen sources: anthropogenic emissions from fossil fuel combustion (22.4 Tg N/yr), aircraft traffic (0.45 Tg N/yr), soil-biogenic emissions (5.0 Tg N/yr), injection of stratospheric NO_x (0.65 Tg N/yr), biomass burning (7.8 Tg N/yr), and lightning discharge (4.0 Tg N/yr) [*Kasibhatla et al.*, 1991; *Kasibhatla*, 1993; *Kasibhatla et al.*, 1993; *Yienger and Levy*, 1995; *Levy et al.*, 1999]. Of these NO_x sources, the GCTM's lightning [*Levy et al.*, 1996] and biomass burning [*Galanter et al.*, 2000] have their greatest influence in the tropics and subtropics. The nitrogen chemistry is precalculated from monthly mean fields, and the lack of synoptic-scale feedbacks is discussed by *Levy et al.* [1999].

The GCTM global distribution of CO is described by *Holloway et al.* [2000]. The simulation included the following as global sources: biomass burning (748Tg CO/yr), fossil fuel combustion (300Tg CO/yr), biogenic hydrocarbon oxidation (683 Tg/yr), and CH_4 oxidation (758 Tg CO/yr). The only CO destruction pathway is OH oxidation based on precalculated monthly mean three-dimensional OH fields [*Spivakovsky et al.*, 1990] that have been scaled by 1.15 to match the observed CH_3CCl_3 global lifetime of 4.8 years. We do not expect their use to significantly affect either the mean or synoptic behavior of CO which has a chemical lifetime of weeks.

3. Model Evaluation

Before presenting a detailed analysis of the transport and chemistry of the SAO ozone maximum, it is important to provide a comparison of the GCTM's meteorology and tracer distribution with available observational data. In this section we will compare the model's regional simulation with climatological wind fields, satellite-determined tropospheric column ozone, ozonesonde tropospheric column ozone data and seasonality at three sites (Ascension Island, Natal, and Brazzaville), and regional ozonesonde profiles.

3.1. Wind Fields

The meteorology of the SAO is remarkable in that its circulation provides a year-long regime of subsidence, anticyclonic surface flow, and essentially no precipitation. Figure 1 presents the model wind fields in the upper, middle, and lower troposphere averaged over the months of August, September, and October (the time of maximum biomass burning), in comparison with the mean August-October observations over a 10-year period [*Oort*, 1983]. At the surface the model and observed winds agree quite well. Here the subtropical anticyclone dominates the wind field with strong diffluent flow from just off the African coast northwestward to the ITCZ in the Atlantic Ocean as well as the North African convergence zone (heavy dashed line). In the middle troposphere at 500 mbar both flow fields are quite weak in the tropics and generally show strong midlatitude westerlies reversing to equatorial easterlies. The model's westerlies depict more troughing over the ocean with the transition zone of weak anticyclonic winds occurring near 5°S as opposed to the observed 15°S. In the upper troposphere the influence of the westerlies is found farther north than at 500 mbar. A weak trough off of South America and an anticyclone over Africa in both the model and observations act to form a confluent zone over the SAO, indicating possible sinking motion to lower levels.
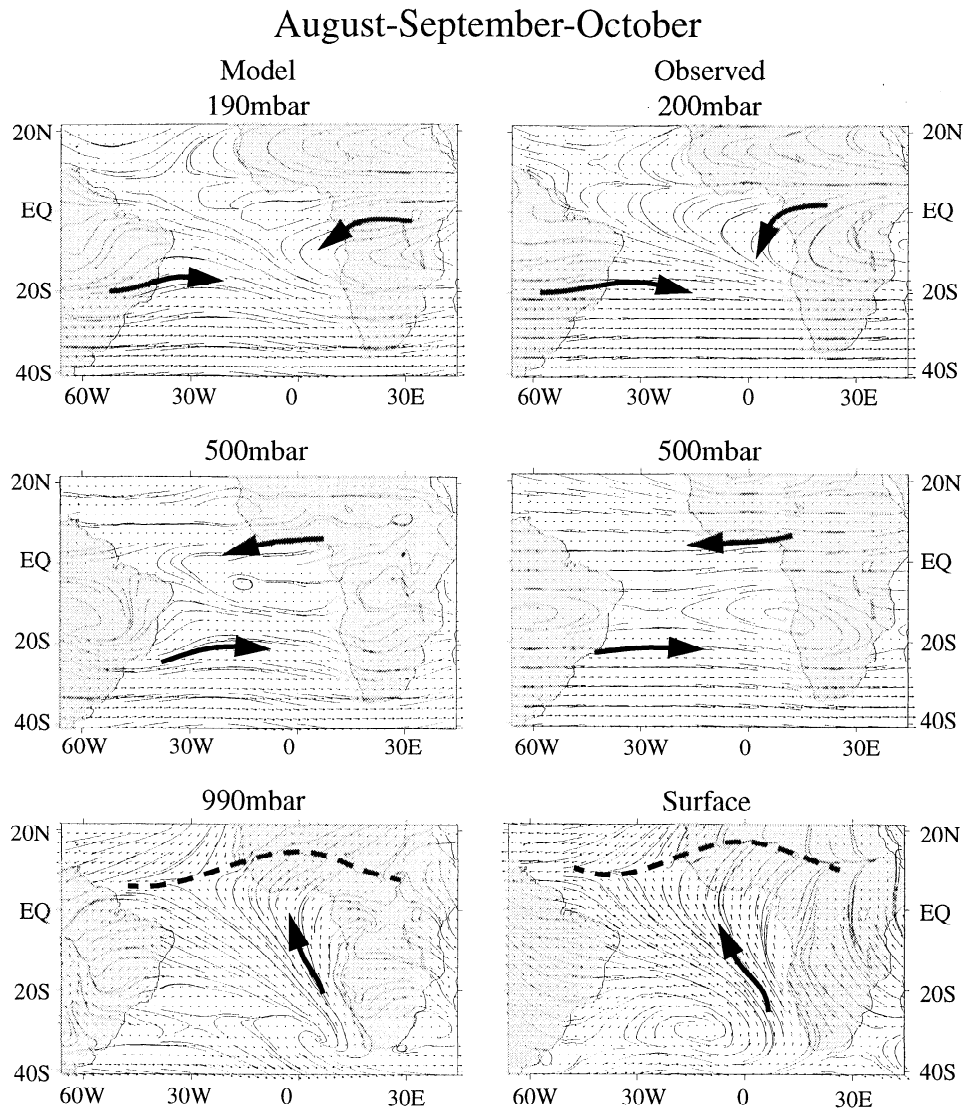
Figure 1. Three-month, time-mean streamlines (August-September-October) for the (left) 190, 500, and 990 mbar model wind fields and the (right) 200 mbar, 500 mbar, and surface observed wind fields. The heavy dashed line represents the ITCZ and the North African convergence zone. The heavy black arrows accentuate the basic flow.

The static nature of this region's circulation can be seen in Figure 2a which depicts the upper troposphere and surface wind fields averaged over March, April, and May, coincident with the seasonal minimum in total tropospheric ozone [*Olson et al.*, 1996]. Once again, the model and observed flow fields agree quite well, and overall the wind fields are very similar to those averaged over August, September, and October. Aloft, the westerlies dominate with a somewhat stronger trough off the east coast of South America, while at the surface, strong anticyclonic flow continues to prevail over the SAO. The only significant seasonal difference is the location of the ITCZ which is found farther south during the Northern Hemisphere (NH) spring.

Since the wind fields of the two seasons are so alike, one would expect the vertical motion over the SAO also to be alike. In Figure 2b we emphasize the SAO by shading only regions of GCTM sinking motion and note that the months of September and April both exhibit similar strong sinking over the subtropical and tropical ocean at 773 mbar, associated

with the surface diffluent zone displayed in both the observed and simulated horizontal flow fields. This same general subsidence pattern extends into the upper troposphere. In general agreement with *Krishnamurti et al.* [1993, 1996], the entire SAO exhibits monthly mean sinking values greater than 0.3 cm/s with values greater than 0.6 cm/s over the eastern half (0.6 cm/s, ~0.5 km/d), while local areas averaged over a shorter time period (5 days) can depict sinking motions of 1.5 to 2.0 cm/s, which can move air 6.5 km to 8.5 km from the upper troposphere to the lower troposphere in approximately 5 days. One should note that the continents exhibit general rising motion for both September and April due to diurnal heating; however, areas of strong upward motion (not contoured) produced by moist convection do migrate with the seasons as does the oceanic rising motion associated with the Atlantic Ocean ITCZ.

Overall, an examination of the area's observed and model wind fields suggests that the basic climatological circulation accumulat⁓ nass over the SAO due to convergence aloft, ex-
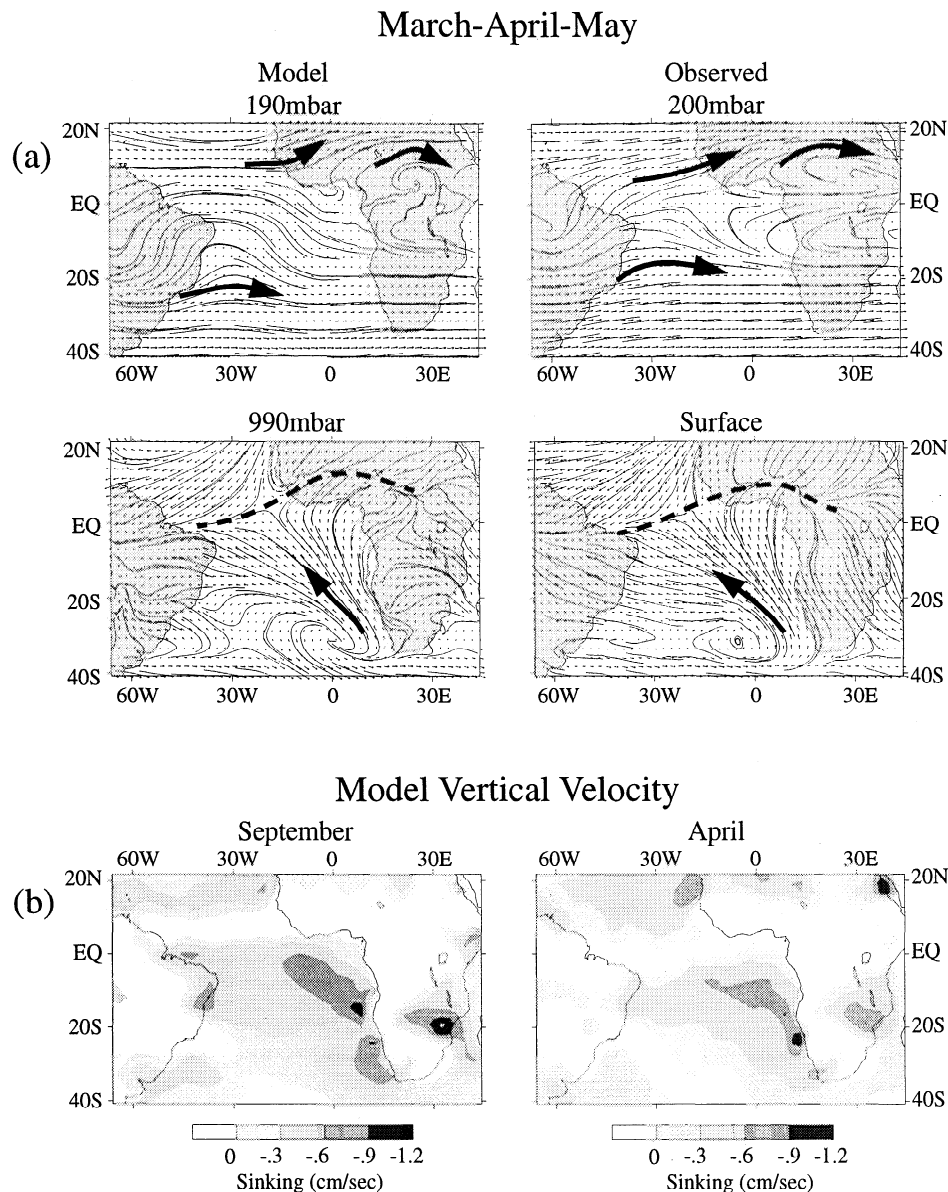
March-April-May

Figure 2. (a) Three-month, time-mean streamlines (March-April-May) for the (left) 190 and 990 mbar model wind fields and the (right) 200 mbar and surface observed wind fields. The heavy dashed line represents the ITCZ and the North African convergence zone. The heavy black arrows accentuate the basic flow. (b) Model vertical velocity (cm/s) at 773 mbar for September and April. Shaded areas represent sinking motion, and the white area (no contour intervals) represents general rising motion.

hibits subsidence into the lower troposphere, and maintains a divergent anticyclonic surface flow.

3.2. South Atlantic Ocean Tropospheric Column Ozone Maximum

The work of *Fishman et al.* [1990] was the first to exhibit the now well known tropospheric column ozone maximum over the SAO associated with regional biomass burning during the dry season. Their original figure depicted average values greater than 40 DUs during September through November. Since then, various other techniques and refinements have been presented [e.g., *Kim et al.*, 1996; *Fishman and Brackett*, 1997; *Hudson and Thompson*, 1998; *Ziemke and Chandra*, 1998; *Ziemke et al.*, 1998], and while the location of the SAO maximum and the basic horizontal gradients

have not changed, the magnitude of the tropical total column ozone has fluctuated somewhat, ranging from *Fishman and Brackett*'s [1997] revised values of 35 to 40 DUs for September through November up to 45 to 50 DUs presented by *Ziemke et al.* [1998] during September and October 1996.

In our GCTM the 110 mbar level (81-150 mbar) values are always in the stratosphere restricting the model tropopause to 150 mbar in the tropics. Owing to the model's relatively course vertical resolution, grid boxes outside the tropics at any given time can have a tropopause of either 150 or 241 mbar. Since we are interested in DU gradients, we choose to define stratospheric air based on the ozone mixing ratios at a given model level, and after examining numerous ozone-sondes, we define air containing values of less than 100 ppbv as tropospheric. On the basis of this the tropopause is deter-

mined to be either 150 or 240 mbar at each grid box after every 6 hours of model integration, and the tropospheric ozone column is calculated using the appropriate mixing ratios. Averaged over a given month, this provides a smooth poleward transition of column ozone values which incorporates lower tropopause heights and longitudinal ozone variations due to transient weather systems. It should be noted that over the tropical SAO the observed tropopause is usually found near 100 mbar [*Olson et al.*, 1996]. However, an analysis of ozonesonde data at Samoa (14°S) by *Folkins et al.* [1999] showed that the chemopause (the onset of strong ozone vertical gradient) occurs at a lower altitude (14 km) which corresponds well with our model 150 mbar level, and they further speculate that this may apply throughout the oceanic tropics.

Plate 1a displays the GCTM tropospheric column ozone during the month of September when the SAO values are at the maximum. An extensive portion of the SAO is covered by values greater than 37.5 DU with a maximum greater than 42.5 occurring just off the west African coast near 10°S. This compares well with satellite-derived observations in both magnitude and location. Also, in good general agreement with *Ziemke et al.* [1998], an axis of locally high DUs is seen from Brazil eastward to the African coast, as well as a second axis from central Africa southeastward to Madagascar (dashed lines). It is interesting to note that the area of DUs larger than 40 corresponds nicely to the anticyclonic diffluent surface flow and vertical velocity pattern seen in Figures 1 and 2b, respectively, suggesting a probable role for subsidence and/or surface transport from Africa in the accumulation of SAO ozone.

3.3. South Atlantic Ocean Tropospheric Column Ozone Seasonal Amplitude

As part of the TRACE-A campaign, *Olson et al.* [1996] produced a detailed analysis of tropospheric column ozone derived from ozonesonde data at three sites: Natal, Brazil (5°46'S, 35°15'W), on the northeastern coast of South America; Ascension Island (7°57'S, 14°22'W), in the SAO midway between Africa and South America; and Brazzaville, Congo (4°14'S, 15°14'E), near the west coast of Africa. In order to define a statistically significant seasonal amplitude they had to group the data into a larger population so that March through May defined the seasonal minimum, while the maximum was determined to be August through December for Natal, July through October for Ascension Island, and June through September for Brazzaville. For our GCTM, which has data available every 6 hours at all grid points, we selected the maximum and minimum month for the grid box containing the ozonesonde station. To produce a more consistent comparison with the ozonesonde analysis, we chose to integrate our column ozone from the surface to the 100 mbar observed average tropopause height of the stations. This was done by integrating our highest tropospheric layer from 242 to 100 mbar instead of the standard layer of 242 to 150 mbar while assuming a constant ozone mixing ratio given by the 190 mbar value. The resulting DU increase is approximately 7%.

Table 1 summarizes the comparison of model and observations. We first note that while our model annual means are too low by 2 to 4 DUs, Natal produces the lowest tropospheric column ozone, and this result is also seen in the seasonal maximum and minimum values. In general, the seasonal model DUs at Ascension Island and Brazzaville are reasonable although we find slightly higher values at Ascension Island than at Brazzaville, while the opposite is true for the observations. In addition, the standard deviations during the seasonal maximum are comparable; however, the GCTM produces higher standard deviations for the seasonal minimum at Natal and Brazzaville. The model seasonal amplitudes (seasonal maximum minus seasonal minimum) are ~25% smaller than the station values at Natal and Ascension Island, while being nearly the same at Brazzaville. As calculated by *Olson et al.* [1996], the seasonal amplitudes of 10-12 DU produced by the satellite TOR method over the SAO also underestimate the ozonesonde results but agree with our GCTM.

Thus far we have only examined the seasonal behavior of the total tropospheric column. To determine if the seasonality is controlled by the upper troposphere or the lower troposphere, we present in Table 1 the ratio of the 600 mbar to the surface seasonal amplitude to the tropospheric column seasonal amplitude at each site. The GCTM and observations are in good agreement and show that the lower troposphere is most dominant at Brazzaville, downwind of the African burning region. In contrast, Ascension Island has nearly equal contributions from the upper and lower troposphere, while the seasonal signal at Natal is largely driven by the upper troposphere. Even this limited examination of the vertical structure of the seasonal amplitude shows the complex nature of this region, where two continental sites on opposite sides of the SAO and both near biomass burning areas display contrasting behavior for the upper and lower troposphere.

For a more in-depth view of the GCTM's seasonality in the SAO region, Plate 1b presents tropospheric column ozone versus time from 30°S to 15°N along longitude 1.2°W which intersects the center of the September maximum. Overall we note four general impressions and their possible implications: (1) There is a maximum present over the SAO throughout the year varying from a low less than 35 DUs in May to a high greater than 42.5 DUs in September. This is in harmony with the region's transport meteorology exhibiting minimal changes from season to season. (2) Focusing on the time frame from the seasonal minimum to the maximum, the ozone maximum varies in latitude (dashed line), moving north to near 3°S from May through July and then south to 8°S in September. This may be an indication of ozone and/or its precursors arriving from different regions and/or sources at different times. (3) An axis of tropospheric ozone maximum (dashed line) extends poleward through the subtropics during the austral winter. This is a time of active SH midlatitude cyclones and may be indicative of ozone from stratosphere-troposphere exchange processes being transported equatorward in subsiding air and enhancing ozone in the southern SAO as shown by *Loring et al.* [1996]. (4) There is a secondary tropospheric column ozone SAO maximum in February coinciding with biomass burning in North Africa indicating possible cross-equatorial transport of ozone.

3.4. Regional Ozonesondes

The relatively good agreement between model and observed tropospheric column ozone suggests that the features in the data are most likely due to the larger-scale circulation which the GCTM can adequately resolve, as well as the fact that column ozone masks the vertical gradient. This section examines available ozonesondes which display the more complex vertical structure of ozone. The observed profiles are di-

Tropospheric Column Ozone
September
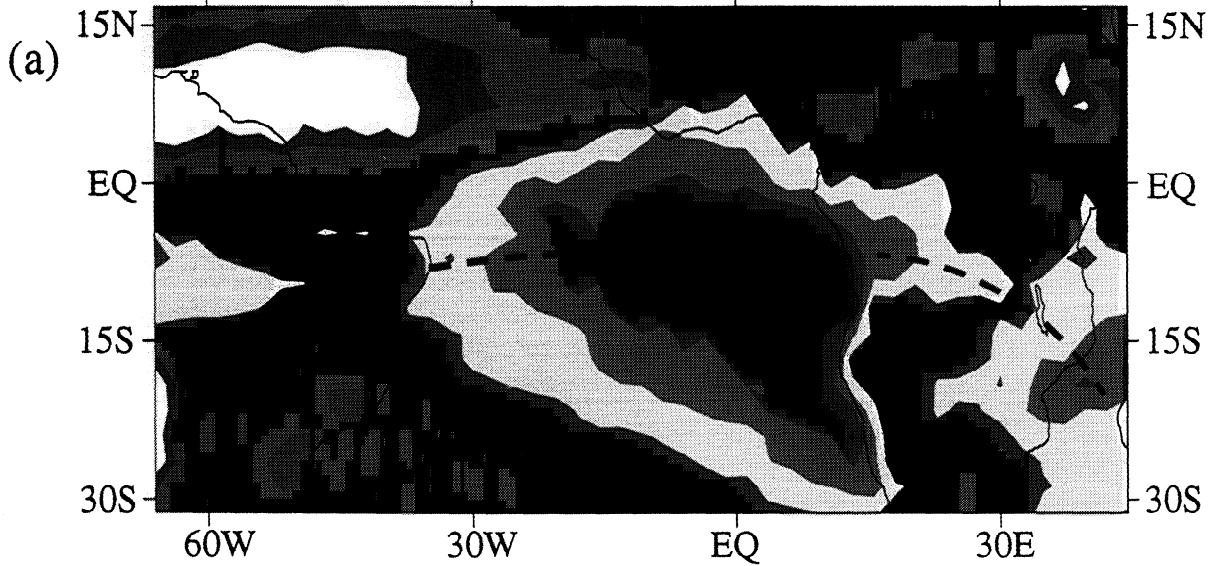
Tropospheric Column Ozone Versus Time
1.2°W
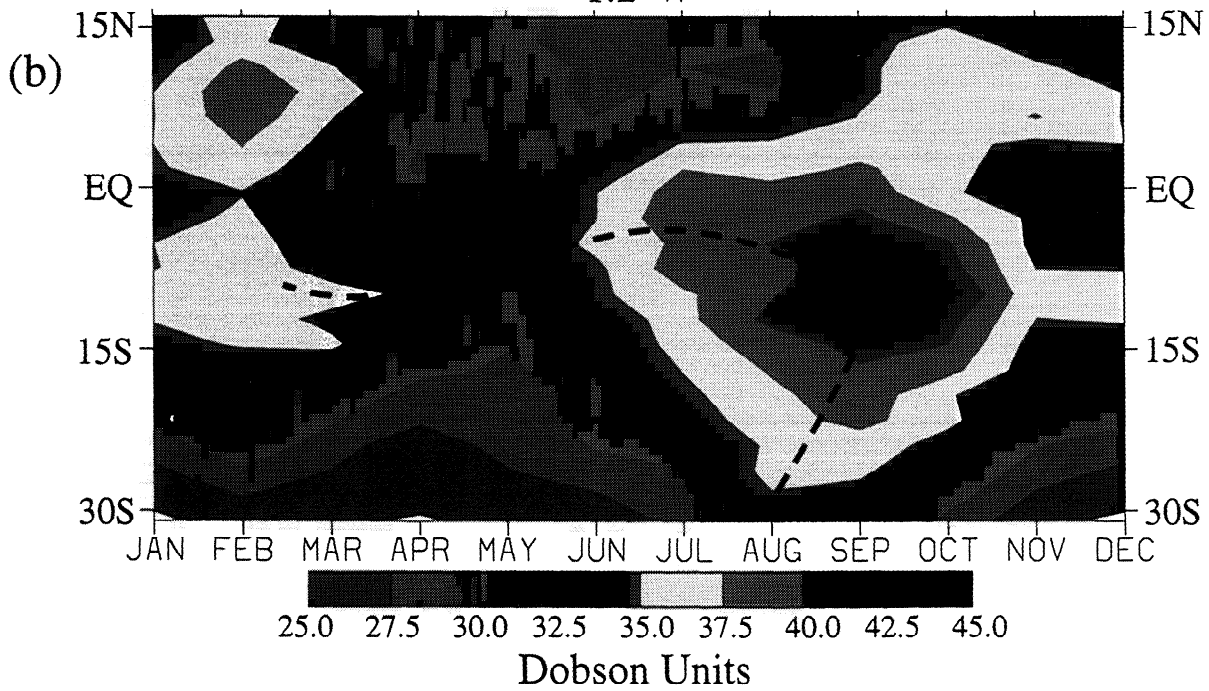
Dobson Units

Plate 1. (a) September tropospheric column ozone (Dobson units). (b) Tropospheric column ozone (Dobson units) versus time at 1.2°W. The dashed lines depict relative maximums.

Table 1. Tropospheric Column Ozone

Sites	Ozonesondes (Integrated to Tropopause)	GCTM (Integrated to 100 mbar)
	Annual Mean	
Natal	36	34
Ascension Island	40	38
Brazzaville	40	36
	Seasonal Maximum (s.d.)	
Natal	43 (9) Aug.-Dec.	38 (8) Sept.
Ascension Island	47 (8) July-Oct.	45 (8) Sept.
Brazzaville	48 (7) June-Sept.	43 (6) Sept.
	Seasonal Minimum (s.d.)	
Natal	28 (9) March-May	27 (15) April
Ascension Island	32 (6) March-May	34 (8) May
Brazzaville	36 (7) March-May	32 (11) April
	Seasonal Amplitude	
Natal	15	11
Ascension Island	15	11
Brazzaville	12	11
	Seasonal Amplitude *600 mbar to the Surface / Total Troposphere*	
Natal	39%	36%
Ascension Island	56%	52%
Brazzaville	60%	61%

rectly affected by diurnal mixing due to solar heating, any intermittent nearby biomass fires, and longer-range transport from ozone precursor source regions, all of which lead to ozone soundings which typically are highly variable in space and time. In a GCTM these processes occur on the subgrid-scale making it difficult to reproduce small-scale features. In particular, our GCTM has no diurnal heating of the BL, emissions from individual fires are distributed uniformly over each 265 by 265 km grid box [*Galanter et al.*, 2000], and its vertical resolution is much coarser than that provided by ozonesondes. However, in general, a GCTM should be able to qualitatively reproduce the basic shape and mixing ratios of the observed profiles.

Figures 3 and 4 depict September ozonesonde and model profiles from South America, Ascension Island, and Africa. Note that some stations present data from only a single year and others present multiple years, while our GCTM represents only one September. Overall, we see that (1) there are two basic types of ozonesonde profiles, those that increase rapidly outside the BL with a slower increase to the tropopause and those that are more vertical in nature (e.g., Cuiaba and Porto National in South America, Etosha in Africa), and (2) the model tends to somewhat underpredict ozone especially in the middle and lower free troposphere.

In more detail, Figure 3 depicts ozonesonde and model profiles in South America and Ascension Island that are presented in rough geographical arrangement. The observed coastal profile at Natal shows a marked increase of ozone with height as compared to the inland profiles at Cuiaba and Porto which are more vertical in nature, perhaps due to unique meteorological conditions during its single year of TRACE-A measurements favoring rapid vertical mixing. At Porto the

ozonesondes capture the high BL levels of ozone produced from nearby fires, while much smaller BL values are observed at Cuiaba. This suggests that the Cuiaba site is farther removed from local biomass burning and in situ ozone pollution production than Porto. The observed BL difference of ozone between these two biomass burning sites accents the difficulty a model has in duplicating NO_x source processes that occur below its resolvable grid scale. In concert with this, the Cuiaba GCTM grid box agrees well with local BL ozonesonde values as well as the column in general, while the model Porto grid box significantly underestimates the lower and midtroposphere values.

At Natal the model produces the general increase with height, but the midtroposphere values are too low due to transport being weak and mostly from nonburning oceanic regions. The observed marine profile at Ascension Island is markedly different from the continental profiles. Low ozone mixing ratios contained in the BL increase rapidly to a midtroposphere maximum near 600 mbar and then decrease slightly to lower values in the upper troposphere. The GCTM's vertical structure also depicts a pronounced rise in ozone above the marine BL. Although the model does not produce the distinct observed maximum in the midtroposphere, its rate of increase with height changes abruptly at 500 mbar and then remains nearly constant through the upper troposphere. We believe the model's inability to capture the 600 mbar maximum is a result of its relatively course vertical resolution. Above the BL at 835 and 685mbar, the general flow to Ascension Island is from the east off of the African coast. The region above the SAO is one of high static stability due to relatively cool BL temperatures resulting from ocean upwelling and relatively warm midtroposphere temperatures resulting from adiabatic

compression due to subsidence. The net affect is that any transported ozone leaving Africa becomes trapped at its exit level above the BL and is then advected along nearly horizontal isentropic surfaces to Ascension Island. The exit level, however, is determined by diurnal convective mixing over the continent which is highly variable in height and time and results in the transport of discreet pockets of ozone constrained in narrow layers. This can be seen by examining individual ozonesondes at Ascension Island which show sharp layers of maximum ozone which vary with height from day to day. Although our GCTM adequately captures the occurrence and height of convective mixing [see *Moxim*, 1990, Table 2; *Levy et al.*, 1999, appendix], the BL values are diffused through relatively large layers (~1.5-2.0 km), reducing distinct maximums of ozone and reactive nitrogen available for horizontal transport.

The African ozonesonde stations and model comparisons are shown in Figure 4, and once again are arranged in rough geographical order with Brazzaville in west tropical Africa, Nairobi in east tropical Africa, Etosha in west subtropical Africa, and Irene in east subtropical Africa. All four sites show a significant increase in ozone above the BL, and this is captured by the model as well as the BL values themselves. In the free troposphere the simulated values overlap with most of the observed ozone data from Nairobi and Irene, and the basic profile shapes are similar, while mixing ratios are too low at Brazzaville and Etosha. The Brazzaville ozonesondes show an upper troposphere maximum near 350 mbar and a possible second maximum at 650 mbar, both of which are accentuated by discrete layers of maximum ozone indicative of transport from the burning regions of interior Africa. These features are not resolved by the model which produces a maximum at 500 mbar. At Etosha the five September ozonesondes from TRACE-A data produce a distinctly different profile from the other African stations and are more representative of Cuiaba and Porto National in South America. Local meteorological conditions may have allowed rapid mixing in nearby biomass burning regions producing a well mixed ozone column which was transported to Etosha.

While ozonesondes provide an accurate detailed picture of the vertical structure of ozone, there is no equivalent for reactive nitrogen profiles. However, a qualitative examination of
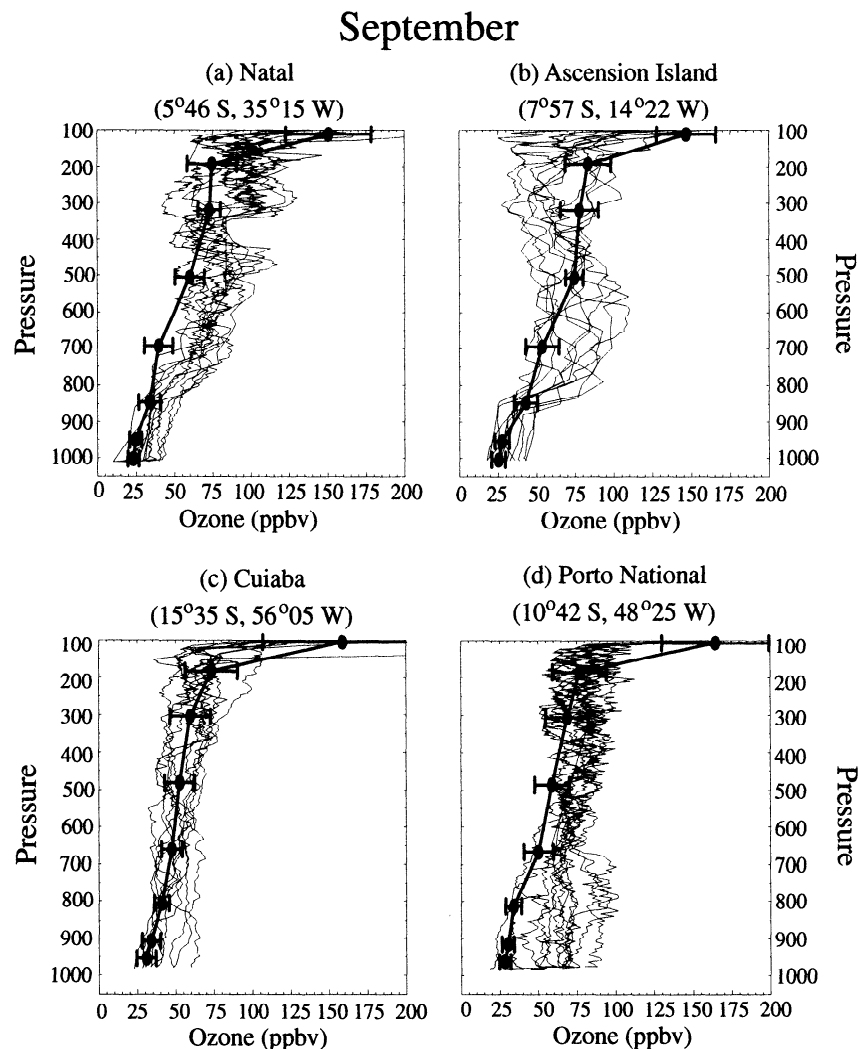
September

Figure 3. September South America and Ascension Island ozonesonde sites and model results. Solid circles are the model mean values with standard deviations, and the thin black lines represent individual ozonesonde profiles. (a) Natal [from *Kirchhoff et al.*, 1996] ("TRACE-A single year"), (b) Ascension Island (NASA/GTE data archive at NASA Langley "multiyear"), (c) Cuiaba [from *Kirchhoff et al.*, 1996] ("TRACE-A single year"), (d) Porto National [from *Kirchhoff et al.*, 1996] ("TRACE-A single year").

September
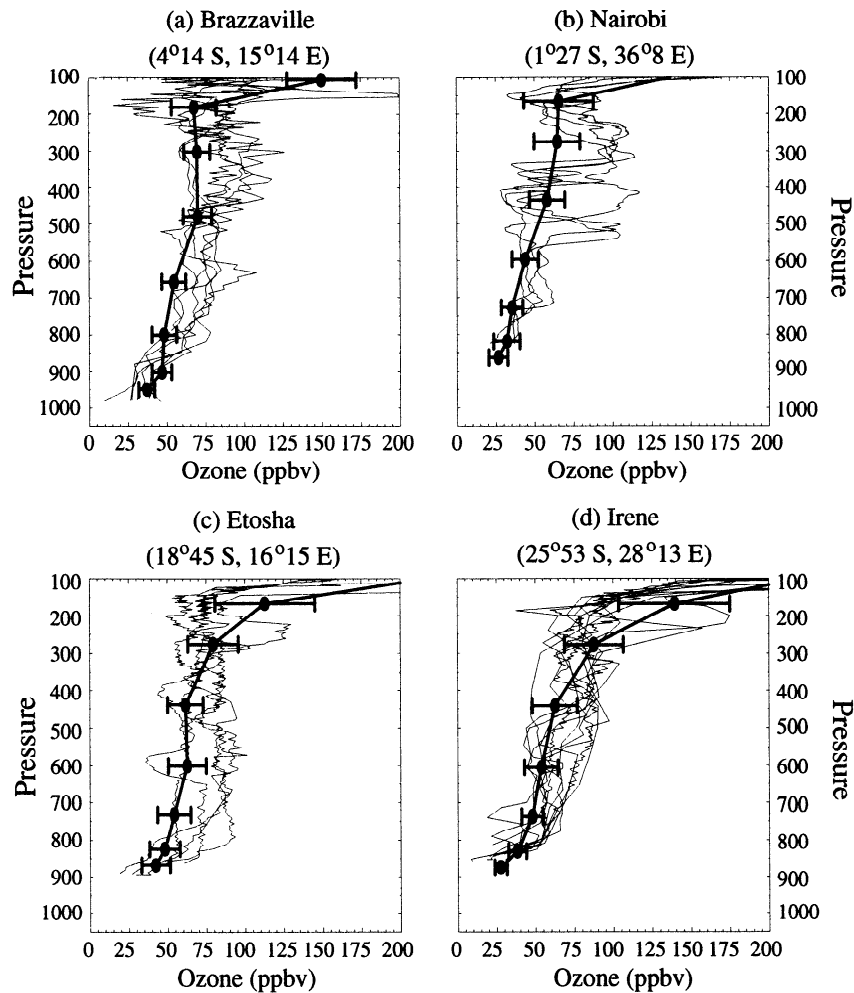
Figure 4. As in Figure 3, except for Africa ozonesonde sites. (a) Brazzaville (NASA/GTE data archive at NASA Langley "multiyear"), (b) Nairobi (Southern Hemisphere Additional Ozonesondes (SHADOZ) "single year"), (c) Etosha (NASA/GTE data archive at NASA Langley "TRACE-A single year"), (d) Irene (J. R. Olson, personal communication, 1998 "multiyear").

the vertical structure of NO_x can be obtained by examining available aircraft measurements over given geographical regions. In Figure 5 we present a comparison of simulated and observed NO_x profiles produced by binning data from TRACE-A flights into our model vertical slabs from three areas, South America, the South Atlantic Ocean, and Africa, where model values are calculated by considering all grid boxes in a given region every 6 hours during the TRACE-A time period (September 23 to October 25).
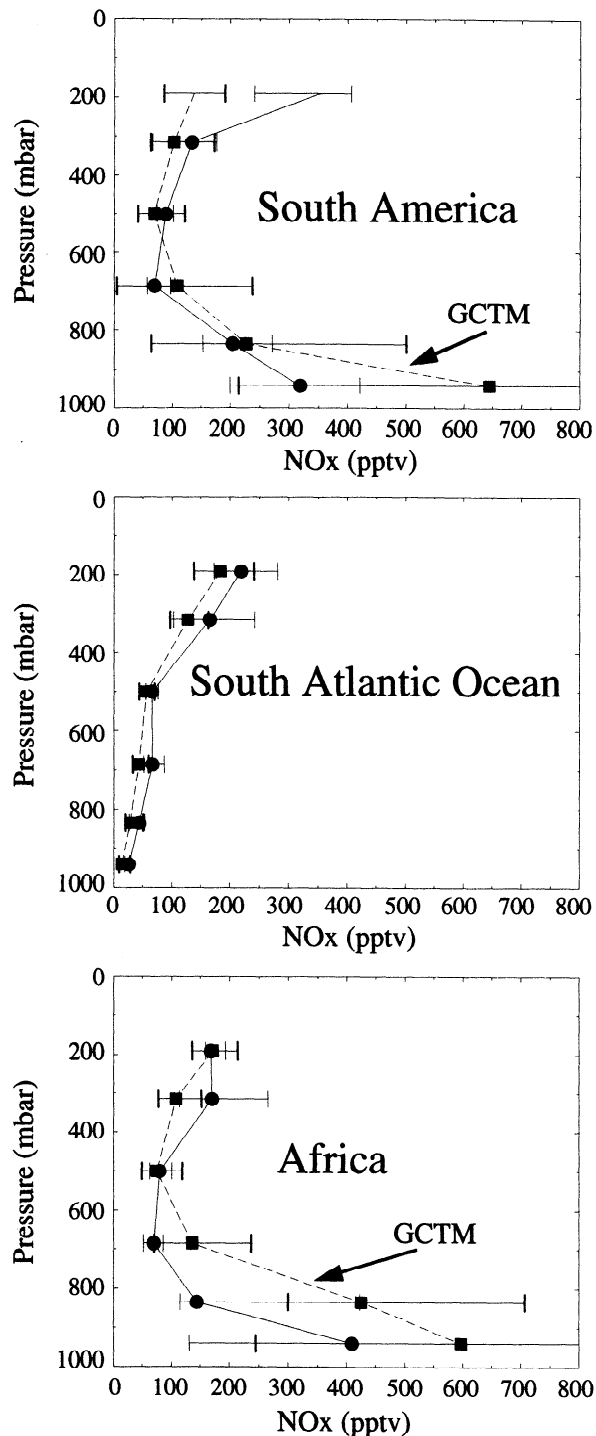
Unlike ozone which essentially always increases with height, NO_x has two distinct vertical structures. Over land there is a "C" shaped profile with a maximum in both the BL associated with continental sources, and the upper troposphere, while the ocean profile is more ozone-like with a minimum in the BL and increasing values with height. The GCTM captures these contrasting shapes, although there are large differences in the continental BL and the upper troposphere over South America (see discussion by *Levy et al.* [1999]). While simulated median NO_x profiles in the TRACE-A region are uniformly lower than the observed, there are strong overlaps between their middle 50% or interquartiles.

4. Model Analysis of the South Atlantic Ocean Ozone Maximum

Using a GCTM, we can theoretically unravel the individual effects of transport and chemistry, although this can be complex at times due to the nonlinear nature of ozone photochemistry. In nature and the model world, transport typically acts to smooth out gradients, while physical sources and photochemical sources and sinks create them. In our GCTM the increase or decrease of mass over time at a given grid box and its relationship to transport and chemistry can be described by a generic mass continuity equation as

$$\frac{\partial}{\partial t}P_sR = -\nabla_\sigma \cdot \vec{V}_2 P_sR - \frac{\partial}{\partial\sigma}\dot{\sigma}P_sR +$$

$$DIFFUSION + CHEM_{source} - CHEM_{sink} \quad (1)$$

where the first two terms on the right side of equation (1) represent horizontal and vertical transport, respectively, and R is the mixing ratio of a given species, V_2 is the horizontal vector wind, ∇_σ is the gradient operator on a surface of constant σ,

In this current study we simplify the analysis problem by choosing a region void of any significant NO_x sources and a time of year (September) when the volume mass of ozone is at a maximum and its time tendency over the month is small. This produces a situation where the most likely scenarios are as follows: (1) the net transport is balanced by the net chemistry; (2) transport is zero, and chemical production (CHEM$_{source}$) equals chemical destruction (CHEM$_{sink}$); or (3) net chemistry is zero, and the horizontal and vertical transport cancel each other. In view of this we perform our analysis of the ozone maximum only over the SAO as depicted by the rectangle in Figure 6, hereafter referred to as the South Atlantic Analysis Region (SAAR), where there are no NO_x sources from biomass burning or other continental sources and only a negligible contribution from lightning. In addition, this region encloses most of the observed and computed tropospheric column ozone maximum. While this area is decidedly smaller than the TRACE-A regional study of *Jacob et al.* [1996], who included the continents of South America and Africa in their work, we feel that our SAAR offers a cleaner analysis uncomplicated by direct ozone precursor sources.

4.1. Simulated Ozone and NO_x Distributions

Figure 7 presents fields of ozone and NO_x for the model month of September in the upper troposphere (315 mbar), the middle troposphere (685 mbar), and the BL (940 mbar). Overall, we see that the vertical structure noted in the observed and GCTM profiles generally applies over the entire region. Ozone values increase everywhere with height. The largest NO_x mixing ratios, however, are located in the continental BL associated with its surface sources and then decrease with altitude until a secondary maximum is found in some areas of the upper troposphere north of surface source regions. In contrast, the NO_x profile over the SAO is one that increases with height similar to ozone.

Upon closer inspection we note that in the BL both ozone and NO_x display a bulge of mixing ratio maxima extending off the west coast of Africa associated with strong low-level southeasterlies shown in Figure 1. At 685 mbar a second tongue of NO_x is observed extending off the east coast of South America associated with free tropospheric westerlies; however, surprisingly, there is no concomitant protrusion of ozone. This result accentuates the complex relationship between gradients, transport, and sources or sinks discussed in the previous section. Strong BL sources of reactive nitrogen over South America provide a sharp vertical gradient allowing rapid mixing of large NO_x mixing ratios into the background troposphere. This influx of NO_x amplifies the horizontal gradient allowing downgradient transport off the coast where it is removed by net chemical destruction. The mean vertical gradient of ozone, however, increases with height reducing the affect of vertical mixing. The larger free tropospheric values of ozone are in part due to vertically transported NO_x providing a chemical source of ozone. More importantly, the downstream tongue of NO_x produces a region of net chemical ozone production which diminishes the horizontal tracer gradient and subsequently reduces the downgradient ozone transport. In the upper troposphere a primary maximum of ozone is isolated over the SAO with large values also found poleward of 25°S presumably associated with midlatitude cyclones [*Loring et al.*, 1996], while the largest values of NO_x are situated over the continents. Overall, ozone throughout the tropo-

Figure 5. Regional vertical profiles of simulated and observed NO_x median values with their interquartile ranges represented by brackets for South America (55°W-35°W, 30°S-5°S), the South Atlantic Ocean (20°W-10°E, 20°S-0°), and Africa (12°E-40°E, 35°S-10°S). The observed data were derived from TRACE-A flights, and model results were taken from grid boxes within the flight domain. The observed profiles are represented by solid circles and solid lines, and the GCTMs are denoted by solid squares and dashed lines.

σ is the vertical sigma velocity ($d\sigma/dt$), P_s is the surface pressure, and t is time. The individual terms of equation (1) can then be averaged over time and integrated over any model domain to produce a budget analysis.
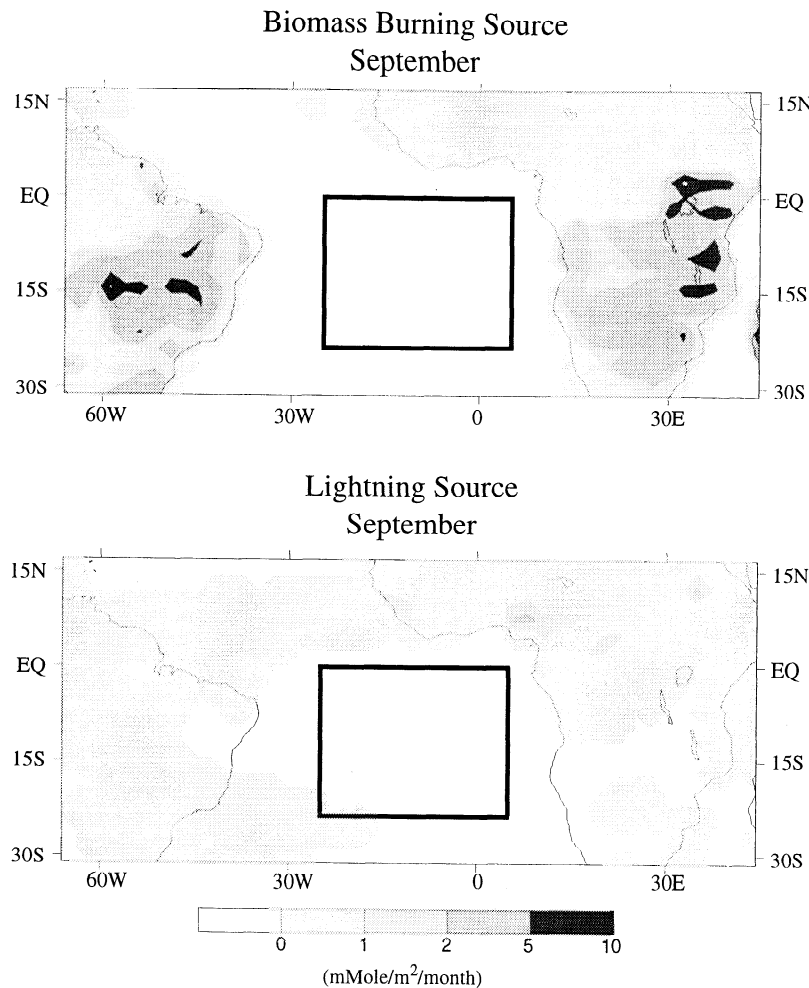
Figure 6. Regional maps of NO_x emissions [mmole m^{-2} month^{-1}] from biomass burning and column-integrated lightning for the month of September. The rectangle represents the South Atlantic Analysis Region (SAAR).

sphere is found to generally increase from the continents to the SAO, while the opposite is true for NO_x even though both undergo identical transport meteorology.

4.2. Vertically Integrated Tropospheric Ozone and The Role of NO_x Sources

Analysis of TRACE-A data has determined that the dominant sources providing NO_x to the SAO troposphere are biomass burning in adjacent Africa and South America, and lightning in the upper troposphere [*Pickering et al.*, 1996; *Smyth et al.*, 1996; *Talbot et al.*, 1996; *Singh et al.*, 1996]. However, the apportionment of each source to the tropospheric mass of NO_x and its affect on background ozone through chemistry could not be established. Utilizing a GCTM, this can be determined by simply removing an appropriate emission from an individual integration. For NO_x, mixing ratios contributed by a particular source are determined by subtracting values generated by a simulation excluding that particular source from mixing ratios simulated using all of the NO_x sources, minimizing any nonlinear effects. The affect on ozone is found by running an experiment with the identical transport meteorology, using NO_x mixing ratios produced with the desired source removed.

We display the monthly volume mass time series of ozone and NO_x computed within the SAAR and integrated from 150 mbar to the surface in Figures 8a and 8b, which show that the September maximum in ozone corresponds to the yearly maximum in total NO_x from all sources (recall that there are no significant reactive nitrogen sources in the region so that all of the NO_x is the result of NO_y transport). An examination of the individual NO_x sources (Figure 8b) indicates that indeed lightning and biomass burning are the largest contributors to total NO_x during September, providing 49% and 36%, respectively, with the remaining 15% produced by the other sources. It is interesting that the lightning NO_x contribution is actually near its minimum, yet in combination with biomass burning produces a maximum. Also, the model produces a secondary maximum in ozone and NO_x in February during the Southern Hemisphere (SH) rainy season associated with a large contribution from lightning and a smaller secondary maximum from biomass burning. The increase in continental lightning during the wet season provides a sharper horizontal gradient in upper tropospheric NO_x, thus augmenting transport to the SAO, while the NO_x from biomass burning, as hinted at in Plate 1b, can only be provided by cross-equatorial transport from the NH as suggested by *Jonquières et al.* [1998].

Within the SAAR it has been shown that volume-integrated NO_x from lightning dominates NO_x produced by biomass burning; however, this may not be true locally when examining their independent effects on tropospheric column ozone. Plates 2a and 2b depict the GCTM tropospheric column ozone fields when the contribution of either biomass burning or lightning NO_x is removed from the ozone photochemical system. A somewhat surprising result is that with biomass burning removed and lightning the controlling NO_x source, there is still a column ozone maximum isolated over the SAO. This suggests that a reduced tropospheric column ozone maximum existed in the SAO prior to the advent of biomass burning by humans. In fact, even the results from a preindustrial ozone experiment [*Levy et al.*, 1997], which included NO_x from only lightning, the stratosphere, appropriately adjusted biogenic release [*Yienger and Levy*, 1995], and a much smaller biomass burning source (10% of present day), showed that a reduced maximum of ~26 DUs was produced over the SAO. This result also accents the role biomass burning plays in the seasonal increase in tropospheric column ozone shown in Plate 1b and is consistent with the results found in the observational study of TRACE-A data by *Mauzerall et al.* [1998].

When lightning is removed, leaving biomass burning as the largest NO_x source (Plate 2b), a closed Dobson maximum is

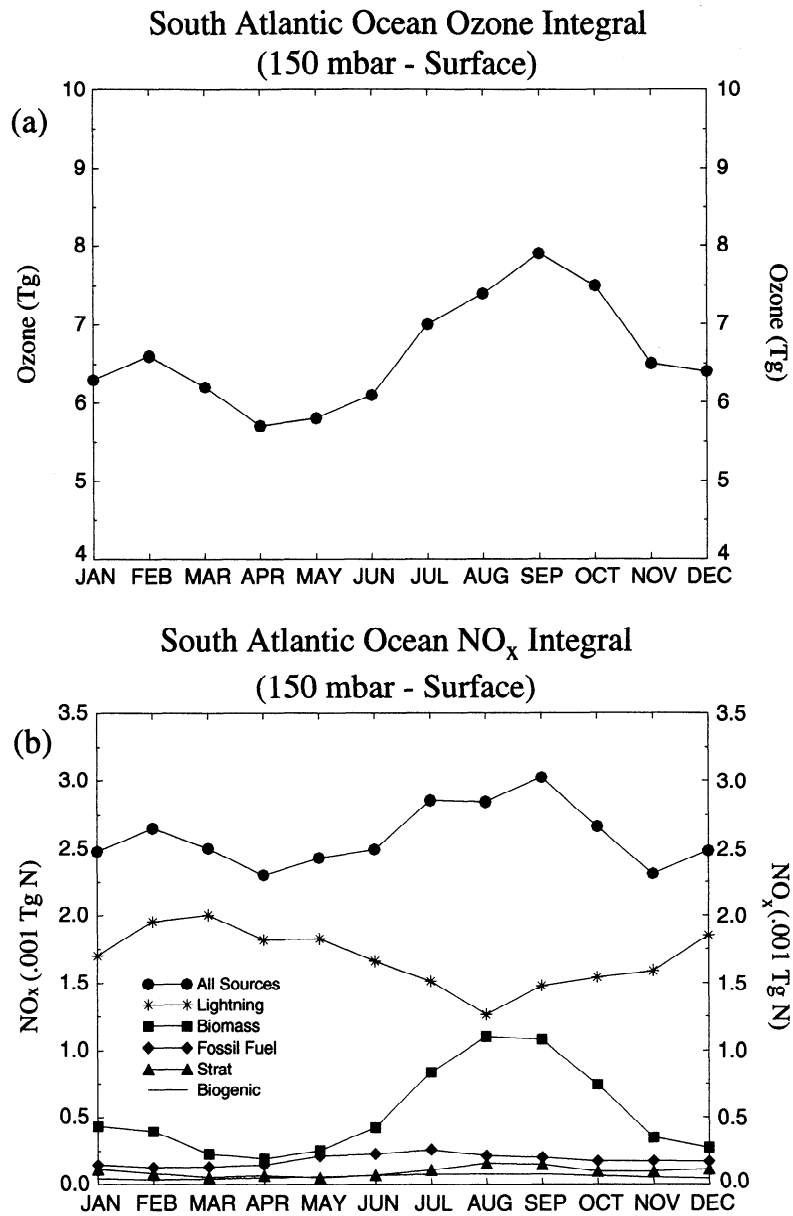once again found over the SAO, but shifted to the south and east relative to Plate 2a. This could imply that the effects of biomass burning NO_x are due to direct transport off of nearby Africa, while the influence of lightning NO_x is associated with subsiding ozone over the central SAO.

4.3. Vertical Structure of Ozone and NO_x

After averaging data within the SAAR at each GCTM level for various ozone and NO_x integrations, Figures 9a and 9b present the vertical distributions of ozone, NO_x, and the influence of NO_x sources. By examining the ozone profile in Figure 9a produced with all NO_x sources included, we see there is a sharp rise in mixing ratios from the low 30s (ppbv) in the BL to the upper 40s (ppbv) at 835 mbar and then to 68 ppbv at 500 mbar with a slower increase at higher levels. The role of biomass burning and lightning in the vertical ozone distribution is depicted by the dashed lines in Figure 9a which show that, while the strongest influence of lightning is in the upper troposphere, the relative importance of biomass burning NO_x to the ozone profile remains remarkably constant from the BL to the upper troposphere. This shows the impact of continental convection mixing ozone precursors aloft where subsequent horizontal transport allows an enhancement of upper tropo-
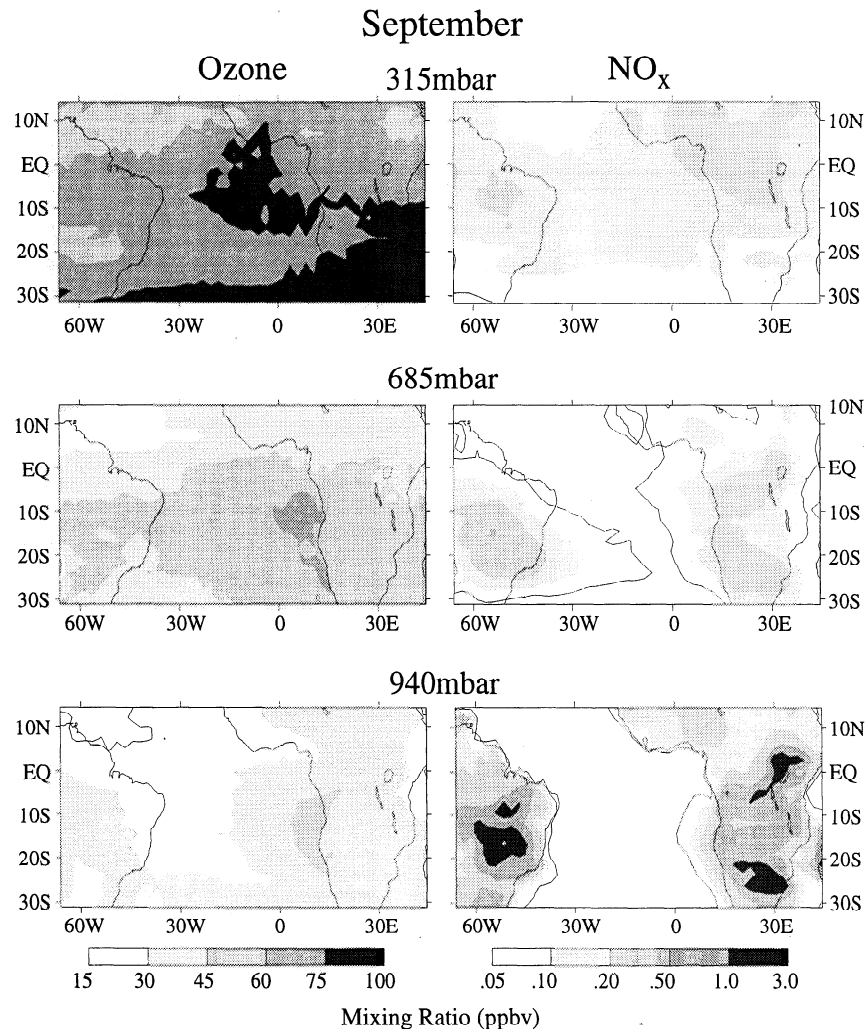
Figure 7. September mean simulated ozone and NO_x mixing ratios (ppbv) at 315, 685, and 940 mbar. Note the different shading scale for each species.

South Atlantic Ocean Ozone Integral
(150 mbar - Surface)

(a)

(Figure 8a: Ozone (Tg) plotted monthly JAN–DEC)

South Atlantic Ocean NO_x Integral
(150 mbar - Surface)

(b)

Legend:
- ● All Sources
- ✱ Lightning
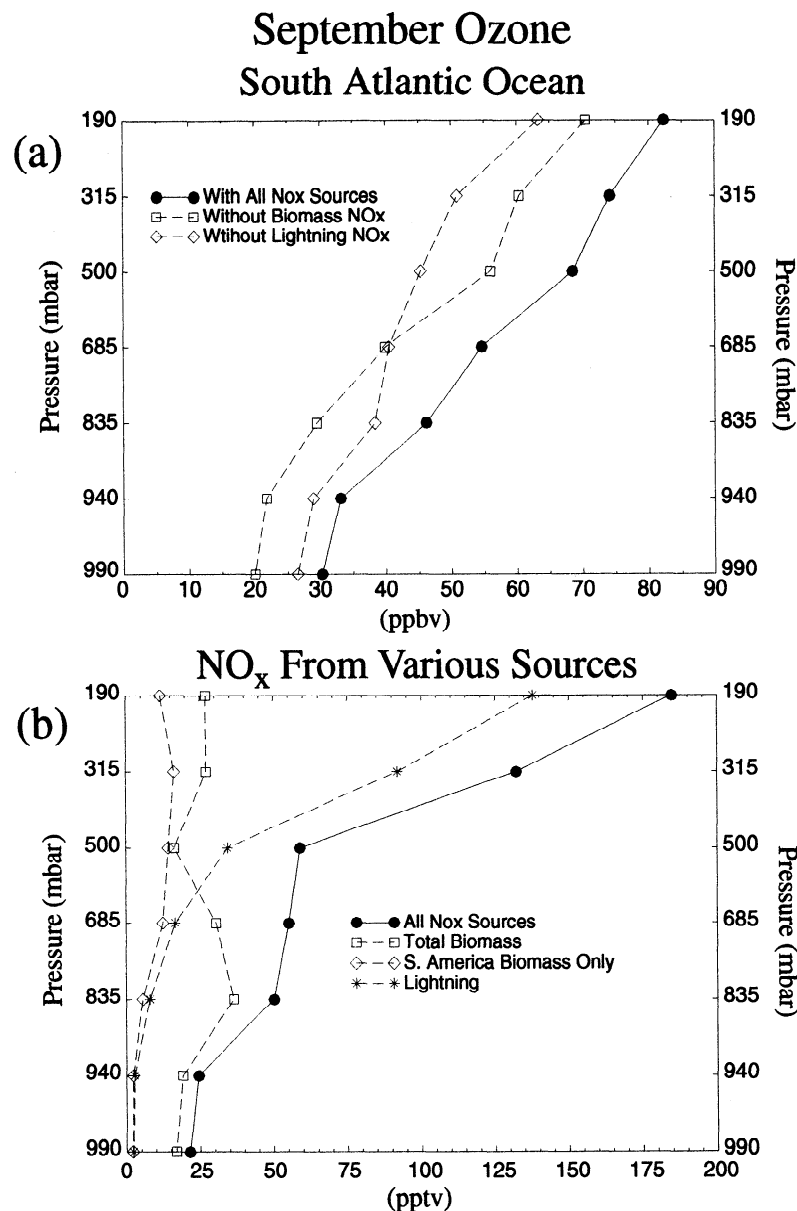- ■ Biomass
- ◆ Fossil Fuel
- ▲ Strat
- — Biogenic

Figure 8. Simulated average monthly mass time series within the SAAR integrated from 150 mbar to the surface for (a) Ozone (Tg) and (b) NO_x (0.001Tg N) from all NO_x sources (solid circles) and the contributions from individual sources (aircraft source is negligible).

spheric ozone in the SAAR, as well as direct low-level transport of pollution ozone and ozone precursors into the SAAR from Africa.

The vertical distribution of NO_x in the SAAR for all sources is shown in Figure 9b, together with contributions from lightning, all biomass burning, and biomass burning without the African contribution. As expected, the high values of NO_x found in the upper troposphere are largely a result of lightning, while NO_x in the lower troposphere originates mainly from biomass burning. The crossover value between the two major sources occurs near 600 mbar at a slightly higher level than the level of equal affect on ozone (685 mbar) seen in Figure 9a. To further dissect the biomass burning contribution to reactive nitrogen, we ran an experiment where its African source was set to zero, but the South American biomass burning (SABB) source remained, allowing us to analyze the rela-

tive importance of each to the SAAR. We first observe that the total biomass burning profile has a primary maximum at 835 mbar, a minimum at 500 mbar, and a secondary maximum in the upper troposphere. By comparing this with the vertical distribution from only SABB, and recalling that there are essentially no NO_x sources emitted in the SAAR, one can obtain an indication of the complex altitude-dependent NO_x transport into this region. At 835 mbar and below, there is little contribution from either lightning or SABB, implying that low-level NO_x is being advected from Africa into the SAAR which would corroborate with the column ozone distribution seen in Plate 2b. In the middle troposphere where lightning and biomass burning have a nearly equal role, we see that SABB increases in importance to essentially dominate the biomass burning effect at 500 mbar, indicative of biomass burning NO_x transport almost solely from South America.

September Ozone
South Atlantic Ocean

NO$_x$ From Various Sources

Figure 9. Simulated vertical profiles averaged over the SAAR for September. (a) Ozone (ppbv) produced with all the NO$_x$ sources (solid circles), with biomass burning removed (open squares), and with lightning removed (open diamonds). (b) Transported reactive nitrogen (pptv) produced from all the NO$_x$ sources (solid circles), from biomass burning only (open squares), from biomass burning without the African contribution (open diamonds), and from lightning (stars).
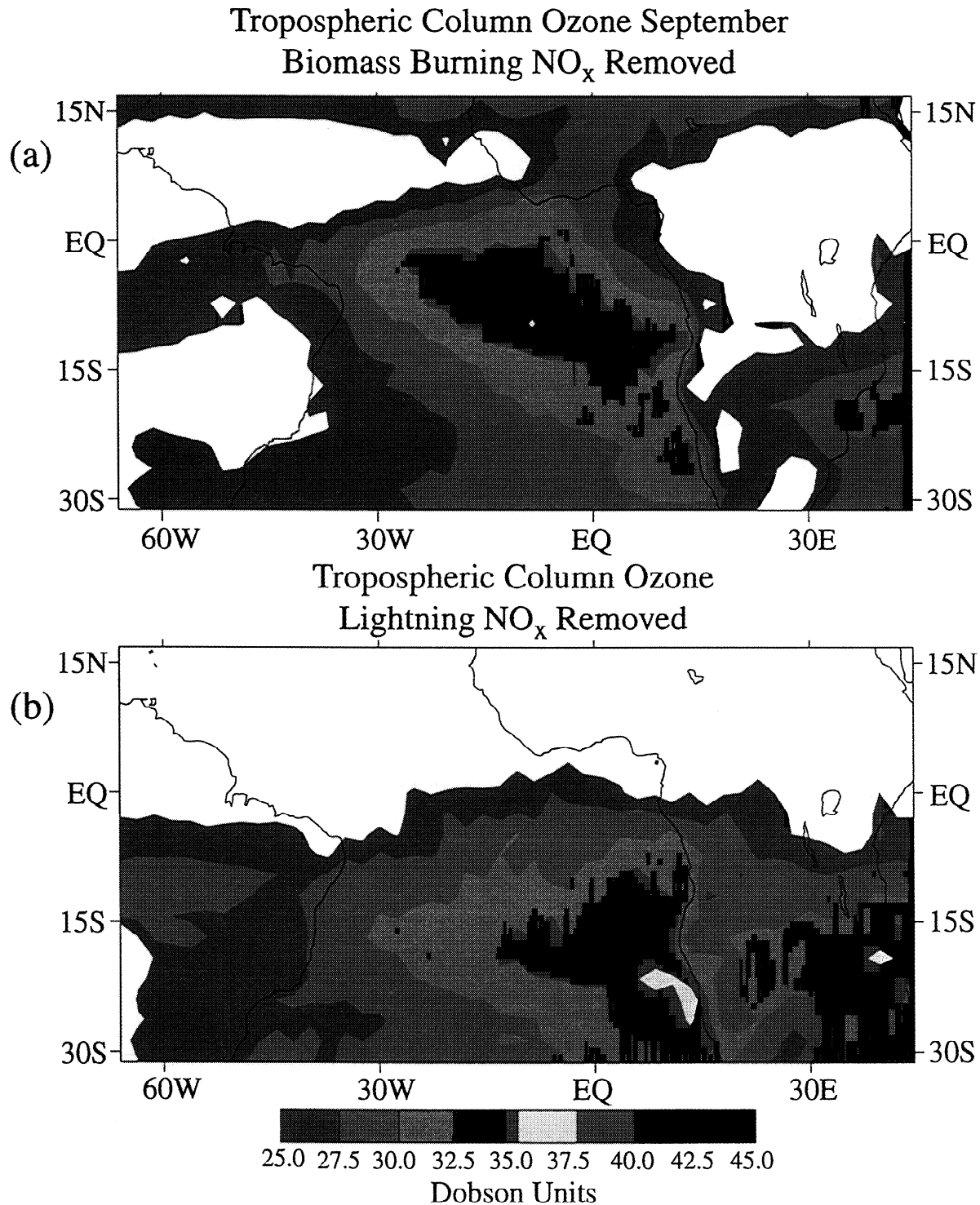
However, the fact that SABB controls roughly 50% of the biomass burning NO$_x$ in the upper troposphere suggests transport to the SAAR from both Africa and South America.

### 4.4. Origin of South Atlantic Ocean Ozone and CO/CH$_4$ Chemistry

One of the fundamental questions raised when one examines profiles of observed or model ozone is, Where did the molecules of ozone really originate? Have they been transported down from the stratosphere or out of the polluted BL, or were they created by CO/CH$_4$ ozone chemistry in the free troposphere and the unpolluted BL? In actuality, a given ozone mixing ratio represents a combination of all three, and it is important to note that biomass burning ozone precursors

contribute to both background CO/CH$_4$ chemistry and pollution chemistry. With available observational data it is impossible to unravel the individual components. However, utilizing a GCTM, it is possible to design an experiment that quantifies these three contributions.

This was accomplished by creating a three-tracer ozone integration, where the source for tracer 1 is the ozone flux from the stratosphere (STRAT), tracer 2 is CO/CH$_4$ chemical production in the background troposphere (CHEM), and tracer 3 is pollution production (POLL). Their chemical sinks are determined by finding the loss rate for the sum of the three tracers and then apportioning it back to each tracer based on the ratio of the individual tracer to the total. The three tracers are then transported independently, and when their sum is com-

Tropospheric Column Ozone September
Biomass Burning NO$_x$ Removed

Tropospheric Column Ozone
Lightning NO$_x$ Removed

25.0 27.5 30.0 32.5 35.0 37.5 40.0 42.5 45.0
Dobson Units

Plate 2. September tropospheric column ozone (Dobson units) produced with (a) biomass burning NO$_x$ removed globally and (b) lightning NO$_x$ removed globally.
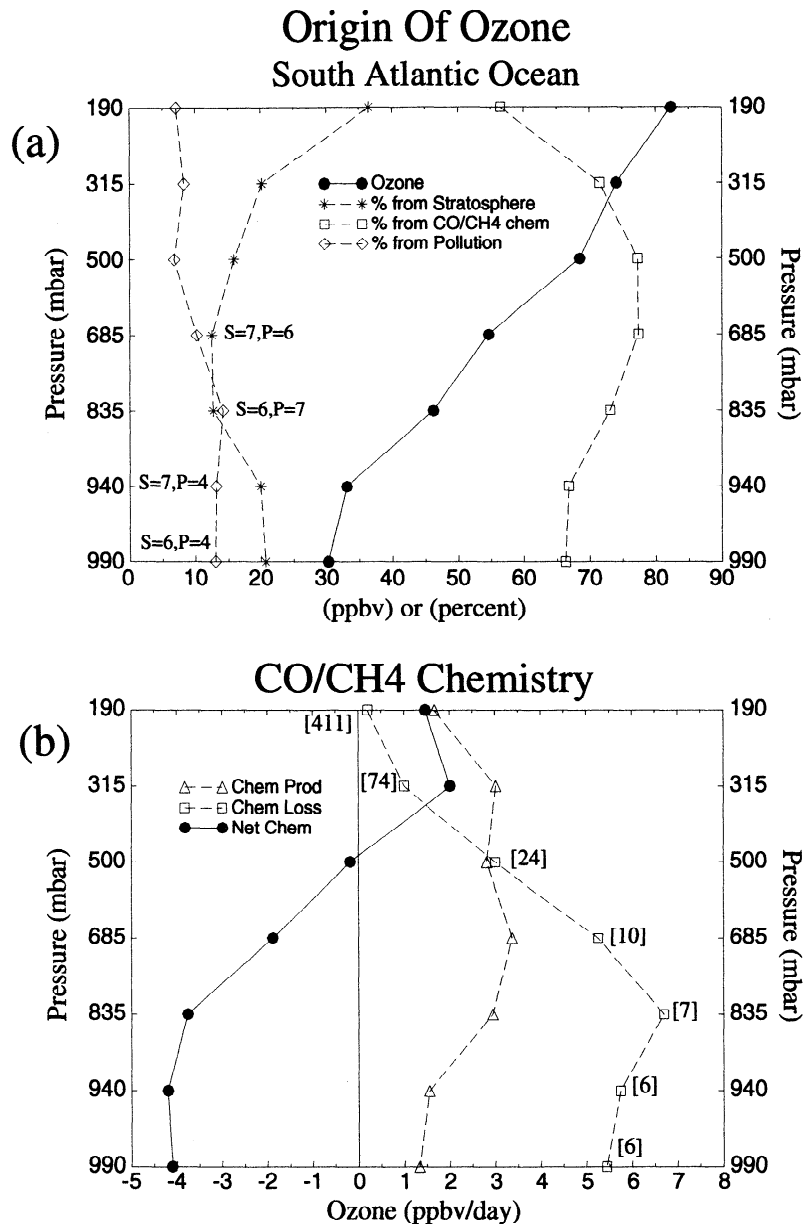
Figure 10. (a) Simulated September vertical profile of ozone (ppbv) averaged over the SAAR (solid circles) and the percent (%) contribution originating from the stratosphere (stars), from background CO/CH$_4$ production chemistry (open squares), and from pollution chemistry (open diamonds). Note that the "S" and "P" represent the actual mixing ratios (ppbv) from the stratosphere and pollution, respectively. (b) SAAR vertical profile of the net (production - destruction) CO/CH$_4$ chemistry (ppbv/d "solid circles"), and the separate production (ppbv/d "open triangles") and destruction rates (ppbv/d "open squares"). The brackets depict the ozone chemical lifetime in days.

pared with the results from the single tracer ozone integration, grid point mixing ratios are within 10%. The discrepancy arises from differences in the gradients between the single tracer experiment and the individual gradients of the three tracer run, and resultant nonlinearities in numerical transport.

The ozone components found in the SAAR are shown in Figure 10a which displays the total ozone mixing ratio profile and the percentage contribution from the STRAT, CHEM, and POLL. Keep in mind that STRAT ozone may have been advected in through the sides of the volume (especially the south side due to midlatitude cyclones) as well as from above, CHEM ozone may have been advected into as well as created

within the volume, and POLL ozone was advected in from the continents. We see that by far CHEM ozone is the main component providing 77% of the ozone in the middle troposphere, 57% at 190 mbar, and 67% in the BL. POLL ozone, while only contributing in the 7 to 14% range, is remarkably consistent with height, indicating both direct low-level transport off of Africa, as well as rapid convective mixing to altitudes where the ozone chemical lifetimes are long followed by subsequent transport away from the continents to the SAO. It is not surprising that the largest contributions from STRAT ozone are in the upper troposphere where air is subsiding directly into the SAAR volume; however, it is curious that it has

a secondary maximum in the BL which is larger than POLL ozone (for convenience the actual mixing ratios are also given in Figure 10a). As a possible explanation, an examination of STRAT ozone revealed that it reached its peak values in the SAAR during late winter (August-September) in association with midlatitude cyclones transporting stratospheric and upper tropospheric air downward and equatorward. An analysis of the latitudinal slope of isentropic surfaces in this region was done to provide an estimate of where air originating in the upper troposphere at high latitudes would enter the SAAR. This revealed that the BL was the preferred location.

Since molecules of ozone provided by CO/CH$_4$ production are the controlling component of ozone within the SAAR, it is important to understand the nature of the background CO/CH$_4$ chemistry itself. Figure 10b depicts the vertical distribution, averaged by level inside the SAAR, of chemical production, chemical loss, and the net. A strong net destruction of ~4 ppbv/d takes place in the BL, which decreases to near zero in the middle troposphere and then changes to a net production of 1.5 to 2.0 ppbv/d in the upper troposphere. This is a result of chemical destruction decreasing from a maximum of ~6 ppbv/d in the BL to less than 1 ppbv/d in the upper troposphere (ozone chemical lifetimes are shown in brackets), while chemical production is more uniform with height, providing 2 ppbv/d in the BL, 3 ppbv/d in the midtroposphere, and decreasing again to less than 2.5 ppbv/d in the upper troposphere.

Unfortunately for model evaluation purposes, the TRACE-A ozone budget analysis by *Jacob et al.* [1996] was produced over a region that included South America and Africa as well as the SAO, and included strong continental BL ozone pollution production in the lower troposphere (0-4 km) not present over the SAO. However, a useful comparison can be obtained by examining their available BL results only over the remote SAO and assuming the budget results in the free troposphere are representative of the SAO. In the SAAR lower troposphere they find a net chemical destruction of ~ -1 to -5 ppbv/d, with +0.3 and +2.1 ppbv/d net chemical production found in the middle (4-8 km) and upper (8-12 km) troposphere, respectively. The observational based chemical production rate shows a middle to upper troposphere decrease from 3.8 to 2.9 ppbv/d, while their chemical destruction rate has a more rapid de-

crease from 3.6 to 0.7 ppbv/d. Overall, this is in good qualitative agreement with our GCTM results.

Also, *Jacob et al.* [1996] used TRACE-A data and a one-dimensional photochemical steady state model to show that the observed ozone profile over their larger analysis volume could be explained by in situ photochemistry, with net production in the upper troposphere being balanced by weak destruction below, suggesting that the horizontal flux divergence is small. However, the ozone profile of our SAAR, uncomplicated by continental meteorology and direct NO$_x$ sources, may be maintained by a different set of controls.

4.5. Ozone and NO$_x$ Budgets

The SAO is a region that appears to accumulate ozone in the upper troposphere through both chemistry and transport. Furthermore, regional subsidence suggests that this buildup of ozone is then transported downward into the lower troposphere where it would be removed by chemical destruction and deposition. While this overall depiction is informative, the qualitative impression needs to be substantiated by a quantitative analysis of the individual processes controlling ozone in the SAAR.

Table 2 depicts the GCTM September SAAR mass budgets of the single tracer ozone experiment (top) and NO$_x$ (bottom) for the entire troposphere, upper troposphere (UT), middle troposphere (MT), and lower troposphere (LT), where each individual term contributing to the monthly mass tendency (see generic equation (1)) is presented (transport: the three-dimensional mass convergence/divergence due to the resolvable wind field, diffusion: three-dimensional mass convergence/divergence due to subgrid-scale processes including dry and moist convection, CO/CH$_4$ net chemistry, pollution chemistry, deposition, and NO$_x$ net chemistry). For ozone we also display the production and destruction apportionment of the net CO/CH$_4$ chemistry, and the mass convergence and divergence components of the transport by the three-dimensional wind field. Note that this is a region where transport due to diffusion is very small so that mass transport is controlled by resolvable grid-scale mass fluxes.

Beginning with an inspection of the entire tropospheric volume (150 mbar to the surface), we see that as expected both ozone and NO$_x$ are being transported into the SAAR. With

Table 2. September Budget of Ozone (Tg O$_3$/month) and NO$_x$ (0.001 Tg N/month)

Budget Terms	150 mbar to the Surface	150-412 mbar	412-773 mbar	773 mbar to the Surface
		OZONE		
Transport	+4.33	-2.17	+1.77	+4.73
Diffusion	+0.00	+0.03	-0.02	-0.01
Net CO/CH$_4$ chemistry	-3.77	2.24	-1.80	-4.21
Pollution chemistry	+0.11	0.00	+0.02	+0.09
Deposition	-0.67	0.00	0.00	-0.67
Mass tendency	-0.03	+0.10	-0.03	-0.10
Production chemistry	10.59			
Loss chemistry	14.36			
Convergence	19.79			
Divergence	15.46			
		NO$_x$		
Transport	+12.82	+3.62	+4.03	+5.17
Diffusion	+0.09	+0.04	+0.09	-0.04
Net chemistry	-12.80	-3.39	-4.15	-5.26
Sources	+0.02	0.02	+0.00	+0.00
Mass tendency	+0.14	+0.29	-0.02	-0.13

ozone the mass convergence due to transport is nearly balanced by net chemical destruction and deposition, and in conjunction with smaller contributions by pollution production and diffusion, results in a near steady state monthly mass tendency of -0.03 (Tg O_3/month). The NO_x transport into the volume is also roughly compensated by its net chemical destruction, and with minor additions by diffusion and a small lightning source, produce a monthly mass increase of +0.14 (.001 Tg N/month). When the transport and net chemistry terms of ozone are decomposed into their individual components (production chemistry, destruction chemistry, mass convergence "total flux in," and mass divergence "total flux out"), we note that for this region, mass convergence of ozone is larger than its chemical production, while mass divergence and chemical loss have essentially the same magnitude.

Further insight into the basic nature of the region can be obtained by examining the UT, MT, and LT profile of the budget terms. We first note that the weak tropospheric mass tendency for both ozone and NO_x actually results from a small mass increase in the UT (150-412 mbar), a very weak decrease in the MT (412-773 mbar), and a small mass decrease in the LT (773 mbar to the surface). A closer inspection of the larger budget terms for ozone and NO_x shows that, while transport is always compensated by net chemistry, the vertical structure of the individual components is somewhat different for each species. For ozone, net chemistry, as shown in mass units here and also depicted in Figure 10b, consists of production in the UT, destruction in the MT, and strong destruction in the LT, while three-dimensional transport is removing mass in the UT and increasing it in the lower levels. In contrast, NO_x mass is being chemically destroyed in each layer volume, and transport is increasing NO_x throughout the troposphere.

Even though the balances of the budget terms are complex, a general picture begins to emerge. In the UT there is a significant September increase in NO_x due to mass convergence by transport exceeding net chemical destruction. In turn, this accumulation of NO_x provides an environment conducive to net chemical production of ozone which is large enough to overcome the ozone evacuation by three-dimensional transport. Ozone in the MT is in near equilibrium with mass transport being balanced by net chemical loss, while in the LT the large three-dimensional mass convergence of ozone actually dominates the strong net chemical destruction; however, the addition of surface deposition produces an overall monthly mass loss.

It is important to note that the budget transport term represents three-dimensional flux convergence/divergence and therefore does not describe the horizontal and vertical flux contributions which play a considerable role in maintaining the regional ozone profile. While our previous analysis has indicated that vertical flux due to subsidence should be important, we need to interpret the mass transport in more detail by examining all the individual flux components.

4.6. Ozone Mass Transport and Circulation

Figures 11a and 11b present the individual flux components comprising the horizontal and vertical contributions to the mass in the full troposphere, UT, MT, and LT volumes where the left column represents the east and west, and upper and lower fluxes (depicted by arrows), and the right column shows the north and south fluxes. It should be noted that since our GCTM solves the mass continuity equation in flux form, our

mass fluxes can be exactly derived (within machine accuracy) from our transport terms (mass convergence/divergence).

We first examine the September mass fluxes (Tg O_3/month) integrated over each face of the entire tropospheric volume (Figure 11a). The largest flux convergence of ozone (12.58) occurs along the E-W axis with the strong west flux in (18.54) being offset by an east flux out. However, the total horizontal flux convergence is reduced to 3.07 as a result of both the north and south fluxes removing ozone. In this volume the vertical flux convergence (+1.26) defines the amount of ozone entering from the stratosphere since the flux is zero at the surface, and while this supplies ~30% of the total mass convergence, the stratospheric flux is small compared to the mass entering from the west.
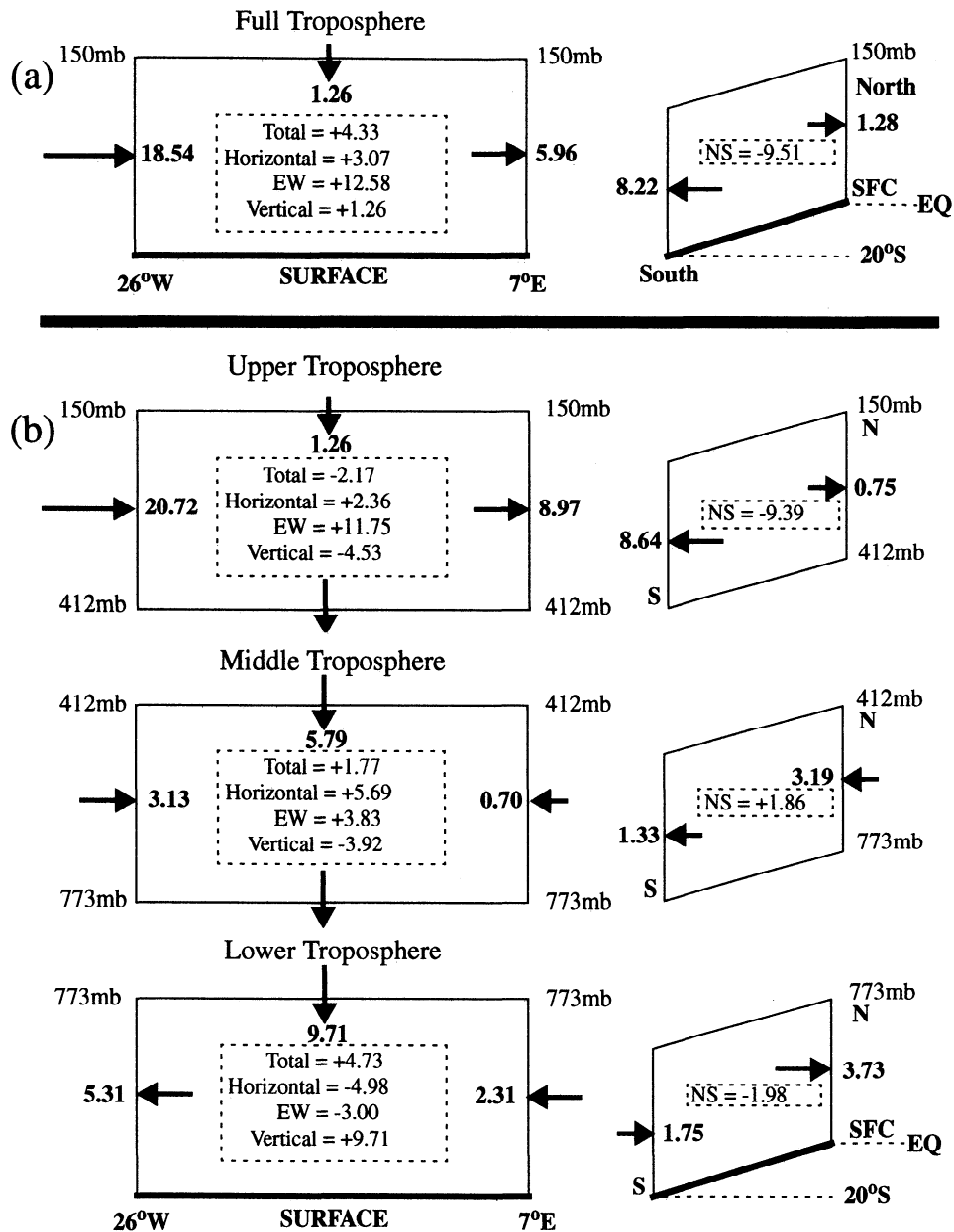
The vertical structure of the mass transport (Figure 11b) verifies the substantial role that descending air plays in the distribution of ozone in this region. In the UT, where our budget analysis demonstrated that chemical production (+2.24) was being offset by three-dimensional transport, we now see that horizontal flux convergence (+2.36) is actually working in concert with chemistry, while a strong vertical flux evacuates the accumulating ozone downward. In the MT, horizontal flux convergence is still occurring and dominates the vertical flux divergence; however, the largest flux component is the downward transport to the LT (9.71). It is this robust subsidence into the LT which surprisingly overwhelms the horizontal mass divergence to produce the total three-dimensional mass convergence discussed in our budget examination. We now see that in addition to net chemical destruction and deposition removing ozone in the LT, both the E-W and N-S components of the horizontal fluxes also are removing mass.

Furthermore, it should be pointed out that the mass transport structure of NO_x (not shown) also shows a strong downward flux at all levels; however, horizontal mass convergence is taking place everywhere, including the BL where there is a strong flux of NO_x from Africa into the domain. This transport of NO_x converging into the region at all levels acts to enhance chemical production of ozone in the upper troposphere and restrain net chemical destruction in the MT and LT [e.g., *Klonecki and Levy*, 1997]. As presented in Figure 9a, if the continental supply of NO_x is lowered due to a removal or reduction of a source, the horizontal gradients are weakened, reducing the mass flux of NO_x into the SAAR. This, in turn, increases net chemical destruction of ozone, helping to alter its profile appropriately.

5. Summary

Using the GFDL/GCTM, we have simulated a tropospheric column ozone maximum over the South Atlantic Ocean throughout the year and a seasonal maximum in the late SH winter (September) associated with the dry season of South America and Africa and corresponding biomass burning. An evaluation with available meteorological and ozone data justifies our quantitative examination of the simulated transport and chemistry.

The GCTM was in good agreement with observed wind fields throughout the region and reproduced the significant South Atlantic Ocean subsidence found in analyses of observational data. Tropospheric column ozone from ozonesonde data at Natal, Ascension Island, and Brazzaville and from corresponding model grid boxes showed similar results in both magnitude and seasonality, as well as the relative contribution

September Ozone Fluxes (Tg O_3/Month)

(a) Full Troposphere

150mb — 150mb — 150mb
North

1.26
1.28

18.54
Total = +4.33
Horizontal = +3.07
EW = +12.58
Vertical = +1.26
5.96

NS = -9.51

8.22 ← SFC ---- EQ
South -------- 20°S

26°W   SURFACE   7°E

(b) Upper Troposphere

150mb — 150mb — 150mb
N

1.26
0.75

20.72
Total = -2.17
Horizontal = +2.36
EW = +11.75
Vertical = -4.53
8.97

NS = -9.39

8.64 ←
412mb

412mb — 412mb
S

Middle Troposphere

412mb — 412mb — 412mb
N

5.79
3.19 ←

3.13
Total = +1.77
Horizontal = +5.69
EW = +3.83
Vertical = -3.92
0.70 ←

NS = +1.86

1.33 ←
773mb

773mb — 773mb
S

Lower Troposphere

773mb — 773mb — 773mb
N

9.71
3.73

5.31 ←
Total = +4.73
Horizontal = -4.98
EW = -3.00
Vertical = +9.71
2.31 ←

NS = -1.98

1.75 → SFC ---- EQ
S -------- 20°S

26°W   SURFACE   7°E

Figure 11. September ozone mass fluxes over the SAAR (flux in or out depicted by arrows). The left column presents the east and west (E-W), and upper and lower fluxes (vertical), and the right column shows the north and south fluxes (N-S). The dashed rectangles display the mass convergence (positive) or divergence (negative) contributed by the E-W, N-S, and vertical fluxes, where horizontal is equal to E-W + N-S and total is equal to horizontal + vertical for (a) the troposphere (150 mbar to the surface) and (b) the upper troposphere (150-412 mbar), the middle troposphere (412-773 mbar), and the lower troposphere (773 mbar to the surface).

of the upper and lower troposphere to the seasonal amplitude. The magnitude of the model's tropospheric column ozone field was within the range of those found from various satellite retrieval methods, and the associated horizontal gradients compared well. A comparison of the ozonesonde data with the GCTM profiles from its 1 year of integration depicted an overall agreement in the general vertical structure for the area. To clarify the relationship between transport and chemistry, we focused our budget analysis on a domain entirely over the South Atlantic Ocean, a region without significant reactive ni-

trogen sources, and a time period (September) when the ozone mass tendency was near zero.

The tropospheric masses of ozone and NO_x integrated over the South Atlantic Analysis Region (SAAR) were both a maximum during September. In that region, transported lightning NO_x [49%] and biomass burning NO_x [36%] dominated with all other sources providing 15%. An ozone simulation without the biomass burning source was still able to produce a reduced tropospheric column ozone maximum (~35 DU compared to ~43 DU) isolated over the South Atlantic Ocean, sug-

gesting that the ozone maximum existed prior to the advent of biomass burning by humans and is simply enhanced by its addition.

Through ozone photochemistry and transport, the two largest NO_x sources play a strong role in controlling the vertical structure of ozone, with lightning dominating in the upper troposphere, while the relative importance of biomass burning is nearly constant throughout the troposphere. Furthermore, it was shown that biomass burning NO_x in the lower troposphere originated from Africa, while the mid and upper troposphere was supplied by South American burning.

By tagging ozone of stratospheric, CO/CH_4 production, and pollution chemistry origins it was found that nearly 70% of the ozone in the SAAR began as CO/CH_4 production. The gross production rates were ~1.5 ppb/d in the BL, ~3 ppb/d through most of the troposphere and decreased to 1.5 ppb/d at 190 mbar, while net CO/CH_4 chemistry was shown to have a 4 ppb/d loss in the BL, was near neutral at 500 mbar, and changed to a net production of 1.5 to 2.0 ppb/d in the UT.

An ozone budget analysis of the tropospheric SAAR during September demonstrated that net mass transport into the analysis domain (+4.33 Tg) is essentially balanced by net chemical destruction (-3.77 Tg) and deposition (-0.67 Tg). In addition, the mass transport into and the mass transport out of the domain are comparable in magnitude to the chemical production and chemical destruction terms. Separating the volume into the upper [UT], middle [MT], and lower [LT] troposphere revealed that a mass increase in the UT (+0.10 Tg) was counterbalanced by a mass decrease in the MT (-0.03 Tg) and LT (-0.10 Tg).

In the UT, horizontal flux convergence (+2.36 Tg) and net chemical production (+2.24 Tg) both supply ozone to the region which is then evacuated downward by subsidence to the rest of the troposphere. In the MT, net chemical destruction and net flux to the LT offset horizontal mass convergence, while in the LT, chemical destruction, deposition, and horizontal divergence overcome strong subsidence of ozone from above the BL.

While the model's horizontal and vertical resolution is too coarse to reproduce observed small-scale features resulting from individual biomass fires and convective mixing generated by daily BL heating, we do not expect the monthly mean budgets and the resulting conclusions to be significantly affected. Moreover, transport to the SAAR is controlled by large-scale flow that is well represented by the GCTM. In the same manner, we do not expect the lack of chemical feedbacks for CO and NO_x as well as the use of monthly mean OH fields for their chemical loss to significantly affect our conclusions. CO has a chemical lifetime of weeks. While NO_x has a chemical lifetime of 1-3 days, OH and NO_x are positively correlated. This would tend to reduce the amplitude of the NO_x fluctuations, but should not significantly affect the mean response of the ozone chemistry, which is relatively linear over the expected range of NO_x.

References

Andreae, M. O., Soot carbon and excess fine potassium: Long-range transport of combustion-derived aerosols, *Science, 220*, 1148-1151, 1983.

Andreae, M. O., J. Fishman, and J. Lindsay, The Southern Tropical Atlantic Region Experiment (STARE): Transport and Atmospheric Chemistry Near the Equator - Atlantic (TRACE-A) and Southern African Fire-Atmosphere Research Initiative (SAFARI): An introduction, *J. Geophys. Res., 101*, 23,519-23,520, 1996.

Chameides, W. L., and J. C. G. Walker, A photochemical theory of tropospheric ozone, *J. Geophys. Res., 78*, 8751-8760, 1973.

Crutzen, P., The role of NO and NO_2 in the chemistry of the troposphere and stratosphere, *Ann. Rev. Earth. Planet. Sci., 7*, 443-472, 1979.

Fishman, J., and V. G. Brackett, The climatological distribution of tropospheric ozone derived from satellite measurements using version 7 Total Ozone Mapping Spectrometer and Stratospheric Aerosol and Gas Experiment data sets, *J. Geophys. Res., 102*, 19,275-19,278, 1997.

Fishman, J., S. Solomon, and P. J. Crutzen, Observational and theoretical evidence in support of a significant in situ photochemical source of tropospheric ozone, *Tellus, 31*, 432-446, 1979.

Fishman, J., C. E. Watson, J. C. Larsen, and J. A. Logan, Distribution of tropospheric ozone determined from satellite data, *J. Geophys. Res., 95*, 3599-3618, 1990.

Fishman, J., F. Fakhruzzaman, B. Cros, and D. Nganga, Identification of widespread pollution in the southern hemisphere from satellite analyses, *Science, 252*, 1693-1696, 1991.

Fishman, J., J. M. Hoell Jr., R. D. Bendura, R. J. McNeal, and V. W. J. H. Kirchhoff, NASA GTE TRACE A Experiment (September-October 1992): Overview, *J. Geophys. Res., 101*, 23,865-23,879,1996.

Fishman, J., V. G. Brackett, E. V. Browell, and W. B. Grant, Tropospheric ozone derived from TOMS/SBUV measurements during TRACE-A, *J. Geophys. Res., 101*, 24,069-24,082, 1996.

Folkins, I., M. Loewenstein, J. Podolske, S. J. Oltmans, and M. Proffitt, A barrier to vertical mixing at 14 km in the tropics: Evidence from ozonesondes and aircraft measurements, *J. Geophys. Res., 104*, 22,095-22,102, 1999.

Galanter, M., H. Levy II, and G. R. Carmichael, Impacts of biomass burning on tropospheric CO, NO_x, and O_3, *J. Geophys. Res., 105*, 6633-6653, 2000.

Hauglustaine, D. A., G. P. Brasseur, S. Walters, P. J. Rasch, J. -F. Muller, L. K. Emmons, and M. A. Carroll, MOZART, a global chemical transport model for ozone and related chemical tracers, 2, Model results and evaluation, *J. Geophys. Res., 103*, 28,291-28,335, 1998.

Hoflich, O., *World Survey of Climatology* vol. 15, *Climates of the Oceans: Climate of the South Atlantic Ocean*, edited by H. Van Loon, pp. 14-21, Elsevier Sci., New York, 1984.

Holloway, T. A., H. Levy II, and P. Kasibhatla, Global distribution of carbon monoxide, *J. Geophys. Res.*, in press, 2000.

Hudson, R. D., and A. M. Thompson, Tropical tropospheric ozone from total ozone mapping spectrometer by a modified residual method, *J. Geophys. Res., 103*, 22,129-22,145, 1998.

Jacob, D. J., et al., Origin of ozone and NO_x in the tropical troposphere: A photochemical analysis of aircraft observations over the South Atlantic basin, *J. Geophys. Res., 101*, 24,235-24,250, 1996.

Jonquières, I., A. Marenco, and A. Maalej, Study of ozone formation and transatlantic transport from biomass burning emissions over West Africa during the airborne Tropospheric Ozone Campaigns TROPOZ I and TROPOZ II, *J. Geophys. Res., 103*, 19,059-19,073, 1998.

Kasibhatla, P. S., NO_y from subsonic aircraft emissions: A global three-dimensional model study, *Geophys. Res. Lett., 20*, 1707-1710, 1993.

Kasibhatla, P., H. Levy II, W. J. Moxim, and W. L. Chameides, The relative impact of stratospheric photochemical production on tropospheric NO_y levels: A model study, *J. Geophys. Res., 96*, 18,631-18,646, 1991.

Kasibhatla, P. S., H. Levy II, and W. J. Moxim, Global NO_x,

HNO₃, PAN, and NO distributions from fossil-fuel combustion emissions: A model study, *J. Geophys. Res.*, *98*, 7165-7180,1993.

Kasibhatla, P., H. Levy II, A. A. Klonecki, and W. L. Chameides, Three-dimensional view of the large-scale tropospheric ozone distribution over the North Atlantic Ocean during summer, *J. Geophys. Res.*, *101*, 29,305-29,316, 1996.

Kidson, J. W., Tropospheric eigenvector analysis and the southern oscillation, *Mon. Weather Rev.*, *103*, 187-196,1975.

Kim, J. H., R. D. Hudson, and A. M. Thompson, A new method of deriving time-averaged tropospheric column ozone over the tropics using TOMS radiances: Intercomparison and analysis, *J. Geophys. Res.*, *101*, 24,317-24,330, 1996.

Kirchhoff, V. W. J. H., Are northern hemisphere tropospheric ozone densities larger? *Eos Trans. AGU, 65*, 449, 1984.

Kirchhoff, V. W. J. H., J. R. Alves, F. R. da Silva, and J. Fishman, Observations of ozone concentrations in the Brazilian cerrado during the TRACE-A field expedition, *J. Geophys. Res.*, *101*, 24,029-24,042, 1996.

Klonecki, A. A., and H. Levy II, Tropospheric chemical ozone tendencies in CO-CH₄-NO_y-H₂O system: Their sensitivity to variations in environmental parameters and their application to a global chemical transport model study, *J. Geophys. Res.*, *102*, 21,221-21,237, 1997.

Krishnamurti, T. N., H. E. Fuelberg, M. C. Sinha, D. Oosterhof, E. L. Bensman, and V. B. Kumar, The meteorological environment of the tropospheric ozone maximum over the South Atlantic, *J. Geophys. Res.*, *98*, 10,621-10,641, 1993.

Krishnamurti, T. N., M. C. Sinha, M. Kanamitsu, D. Oosterhof, H. Fuelberg, R. Chatfield, D. J. Jacob, and J. Logan, Passive tracer transport relevant to the TRACE-A experiment, *J. Geophys. Res.*, *101*, 23,889-23,907, 1996.

Levy, H., II, J. D. Mahlman, and W. J. Moxim, Tropospheric N₂O variability, *J. Geophys. Res.*, *87*, 3061-3080 1982.

Levy, H., II, W. J. Moxim, and P. S. Kasibhatla, A global three-dimensional time-dependent lightning source of tropospheric NO_x, *J. Geophys. Res.*, *101*, 22,911-22,922, 1996.

Levy, H., II, P. S. Kasibhatla, W. J. Moxim, A. A. Klonecki, A. I. Hirsch, S. J. Oltmans, and W. L. Chameides, The global impact of human activity on tropospheric ozone, *Geophys. Res. Lett.*, *24*, 791-794, 1997.

Levy, H., II, W. J. Moxim, and P. S. Kasibhatla. Simulated tropospheric NO_x: Its evaluation, global distribution, and individual source contributions, *J. Geophys. Res.*, *104*, 26,279-26,306, 1999.

Lindesay, J. A., M. O. Andreae, J. G. Goldhammer, G. Harris, H. J. Annegarn, M. Garstang, R. J. Scholes, and B. W. van Wilgen, International Geosphere-Biosphere Programme/International Global Atmospheric Chemistry SAFARI-92 field experiment: Background and overview, *J. Geophys. Res.*, *101*, 23,521-23,530, 1996.

Lockwood, J., *World Climatology*, pp. 86-87, St. Martin's, New York, 1974.

Logan, J. A., Nitrogen oxides in the troposphere: Global and regional budgets, *J. Geophys. Res.*, *88*, 10,785-10,807, 1983.

Logan, J. A., and V. W. J. H. Kirchhoff, Seasonal variations of tropospheric ozone at Natal, Brazil, *J. Geophys. Res.*, *91*, 7875-7881, 1986.

Logan, J. A., M. J. Prather, S. C. Wofsy, and M. B. McElroy, Tropospheric chemistry: A global perspective, *J. Geophys. Res.*, *86*, 7210-7254, 1981.

Loring, R. O., H. E. Fuelberg, J. Fishman, M. V. Watson, and E. V. Browell, Influence of a middle-latitude cyclone on tropospheric ozone distributions during a period of TRACE-A, *J. Geophys. Res.*, *101*, 23,941-23,956, 1996.

Machta, L., K. Peterson, N. A. Lieurance, W.D. Komhyr, and W. Bischof, Meteorological observations from the Rockwell polar flight, *Weather*, *24*, 398-409, 1969.

Mahlman, J. D., and W. J. Moxim, Tracer simulation using a global general circulation model: Results from a midlatitude instantaneous source experiment, *J. Atmos. Sci.*, *35*, 1340-1374, 1978.

Manabe, S., and J. L. Holloway Jr., The seasonal variation of the hydrologic cycle as simulated by a global model of the atmosphere, *J. Geophys. Res.*, *80*, 1617-1649, 1975.

Manabe, S., D. G. Hahn, and J. L. Holloway Jr., The seasonal variation of the tropical circulation as simulated by a global model of the atmosphere, *J. Atmos. Sci.*, *31*, 43-83, 1974.

Mauzerall, D. L., J. A. Logan, D. J. Jacob, B. E. Anderson, D. R. Blake, J. D. Bradshaw, B. Heikes, G. W. Sachse, H. Singh, and B. Talbot, Photochemistry in biomass burning plumes and implications for tropospheric ozone over the tropical South Atlantic, *J. Geophys. Res.*, *103*, 8401-8423, 1998.

Moxim, W. J., Simulated transport of NO_y to Hawaii during August: A synoptic study, *J. Geophys. Res.*, *95*, 5717-5729, 1990.

Moxim, W. J., H. Levy II, and P. S. Kasibhatla, Simulated global tropospheric PAN: Its transport and impact on NO_x, *J. Geophys. Res.*, *101*, 12,621-12,638, 1996.

Newell, R. E., and M.-F. Wu, Simultaneous measurements of carbon monoxide and ozone in the NASA Global Atmospheric Sampling Program (GASP), in *Atmospheric Ozone, Proceedings of the Quadrennial Ozone Symposium, Halkidiki, Greece, 1984*, edited by C. S. Zerefos and A. Ghazi, pp. 548-552, D. Reidel, Norwell, Mass., 1985.

Newell, R. E. Climate and the ocean, *Amer. Sci.*, *67*, 405-416, 1979.

Olson, J. R., A study of the mass transport of enhanced continental ozone in the tropics and its impact over the remote Southern Atlantic Ocean, in *Biomass Burning and Global Change*, edited by J. S. Levine, pp.178-192, MIT Press, Cambridge, Mass., 1996.

Olson, J. R., J. Fishman, V. W. J. H. Kirchhoff, D. Nganga, and B. Cros, Analysis of the distribution of ozone over the southern Atlantic region, *J. Geophys. Res.*, *101*, 24,083-24,093, 1996.

Oort, A. H., Global atmospheric circulation statistics, 1958-1973, *NOAA Prof. Pap. 14*, Natl. Oceanic and Atmos. Admin., Rockville, Md., 1983.

Pickering, K. E., et al., Convective transport of biomass burning emissions over Brazil during TRACE-A, *J. Geophys. Res.*, *101*, 23,993-24,012, 1996.

Pratt, R., and P. Falconer, Circumpolar measurements of ozone, particles, and carbon monoxide from a commercial airliner, *J. Geophys. Res.*, *84*, 7876-7882, 1979.

Richardson, J. L., An investigation of large-scale tropical biomass burning and the impact of its emissions on atmospheric chemistry, Ph.D. thesis, Georgia Inst. of Technol., Atlanta, 1994.

Roelofs, G. J., J. Lelieveld, H. G. J. Smit, and D. Kley, Ozone production and transports in the Atlantic region during the biomass burning season, *J. Geophys. Res.*, *102*, 10,637-10,651, 1997.

Seiler, W., and P. Crutzen, Estimates of the gross and net flux of carbon between the biosphere and the atmosphere from biomass burning, *Clim. Change*, *2*, 207-247, 1980.

Singh, H. B., et al., Impact of biomass burning emissions on the composition of the South Atlantic troposphere: Reactive nitrogen and ozone, *J. Geophys. Res.*, *101*, 24,203-24,220, 1996.

Smyth, S. B., et al., Factors influencing the upper free tropospheric distribution of reactive nitrogen over the South Atlantic during the TRACE-A experiment, *J. Geophys. Res.*, *101*, 24,165-24,186, 1996.

Soden, B. J., and F. P. Bretherton, Interpretation of TOVS water vapor radiances in terms of layer-average relative humidities: Method and climatology for the upper, middle, and lower troposphere, *J. Geophys. Res.*, *101*, 9333-9343, 1996.

Spivakovsky, C. M., R. Yevich, J. A. Logan, S. C. Wofsy, M. B. McElroy, and M. J. Prather, Tropospheric OH in a three-dimensional tracer model: An assessment based on observations on CH₃CCl₃, *J. Geophys. Res.*, *95*, 18,441-18,471, 1990.

Talbot, R. W., et al., Chemical characteristics of continental outflow over the tropical South Atlantic Ocean from Brazil and Africa, *J. Geophys. Res.*, *101*, 24,187-24,202, 1996.

Thompson, A. M., K. E. Pickering, D. P. McNamara, M. R. Schoeberl, R. D. Hudson, J. H. Kim, E. V. Browell, V. W. J. H. Kirchhoff, and D. Nganga, Where did tropospheric ozone over southern Africa and the tropical Atlantic come from in October 1992? Insights from TOMS, GTE TRACE-A, and SAFARI 1992, *J. Geophys. Res.*, *101*, 24,251-24,278, 1996.

Yienger, J. J., and H. Levy II, Empirical model of global soil-biogenic NO_x emissions, *J. Geophys. Res.*, *100*, 11,447-11,464, 1995.

Yienger, J. J., A. A. Klonecki, H. Levy II, W. J. Moxim, and G. R.

Carmichael, An evaluation of chemistry's role in the winter-spring ozone maximum found in the northern midlatitude free troposphere, *J. Geophys. Res., 104*, 3655-3667, 1999.

Ziemke, J. R., and S. Chandra, Comment on "Tropospheric ozone derived from TOMS/SBUV measurements during TRACE-A" by J. Fishman et al., *J. Geophys. Res., 103*, 13,903-13,906, 1998.

Ziemke, J. R., S. Chandra, and P. K. Bhartia, Two new methods for deriving tropospheric column ozone from TOMS measurements: Assimilated UARS MLS/HALOE and convective-cloud differential techniques, *J. Geophys. Res., 103*, 22,115-22,127, 1998.

H. Levy II and W. J. Moxim, Geophysical Fluid Dynamics Laboratory, P.O. Box 308, Princeton University, Princeton, NJ 08542-0308. (wm@gfdl.gov)